candidate residues to alanine. By immunoprecipitation assay, we found that the binding of Plk1 was abolished when Thr 1415 is mutated (Fig. 2A). Consistent with this result, a Far-Western analysis revealed that the PBD protein did not bind to the Thr 1415 mutant when the others do (Fig. 2B). These results suggest that the binding of Plk1 to CAP-D3 depends on the phosphorylation of Thr 1415. Interestingly, the Thr 1415 residue appears to be conserved in higher eukaryotes, whereas the other two candidate sites are not (Fig. 2C).

Because phosphorylation of CAP-D3 depends on both Cdk1 and Plk1 (Fig. 1D), we thought one of these kinases might mediate CAP-D3 Thr 1415 phosphorylation, as these kinases are known to mediate phosphorylation of the PBD-binding motif (Elia et al. 2003; Petronczki et al. 2008; Archambault and Glover 2009). Moreover, we found that the amino acid sequence adjacent to Thr 1415 fits the consensus for Plk1, which led us to predict the Ser 1419 site as a target of this kinase (Fig. 2C). To address these possibilities, we generated recombinant polypeptides that encompass these prospective phospho–sites and used them as substrates for in vitro kinase reactions. The phosphorylation of the peptide was readily catalyzed by Cdk1/Cyclin B and Plk1. In these assays, phosphorylation by Cdk1/Cyclin B was significantly suppressed in a peptide bearing the T1415A substitution, and phosphorylation by Plk1 was suppressed in a S1419A peptide, suggesting that Cdk1 and Plk1 can mediate phosphorylation of CAP-D3 on the Thr 1415 and Ser 1419 residues, respectively (Fig. 2D). Notably, in addition to Thr 1415, Ser 1419 or its equivalent site also seems to be conserved (Fig. 2C).

Enrichment of Plk1 on chromosome axes

The biochemical analyses suggest that Plk1 associates with condensin II by binding directly to CAP-D3. To address at which subcellular region this interaction might occur, we revisited the localization of Plk1 by immunofluoresence microscopy using monoclonal antibodies to Plk1, the specificity of which was verified by staining the Plk1-depleted cells with the same antibodies (Supplemental Fig. 4A–C). In addition to the characteristic localization of Plk1 at kinetochores and the central spindle, enrichment of Plk1 was evident on chromosomal axes during the early stages of mitosis (Fig. 3A), as suggested previously (Santamaria et al. 2007). This localization of Plk1 on chromosome arms accordingly colocalized with condensin II (Fig. 3C). Importantly, the localization of Plk1 on chromosomal axes was perturbed in the absence of CAP-D3, while its enrichment at kinetochores and the central spindle was not affected (Fig. 3B). With a closer inspection of chromosome spread preparations, the enrichment of Plk1 to chromosome axes was unambiguously

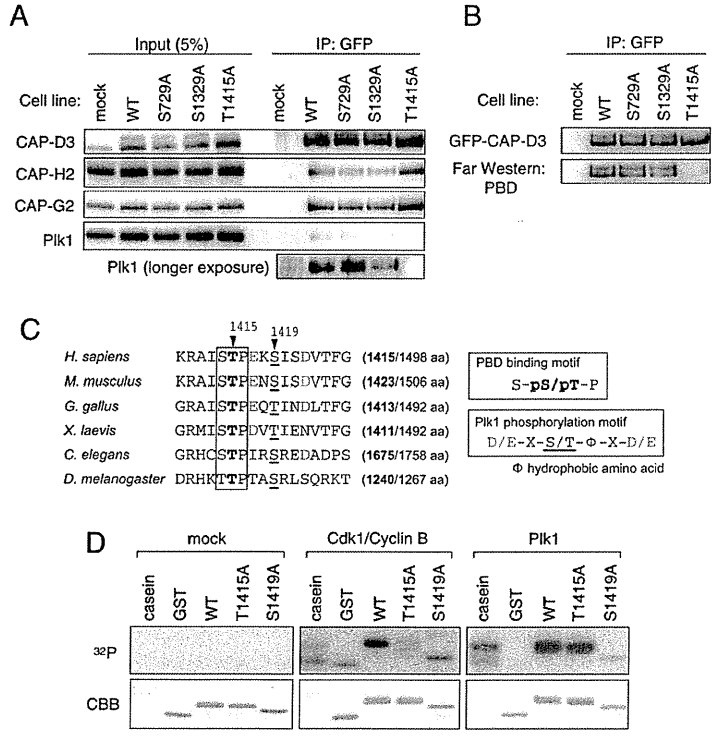

Figure 2. Identification of phosphorylation sites on CAP-D3. (*A*) Immunoprecipitation of Plk1 with CAP-D3 is abolished in a Thr 1415 nonphosphorylatable mutant. Mitotic cell extracts prepared from cells stably expressing the indicated version of GFP-tagged CAP-D3 were subjected to immunoprecipitation analysis with antibodies to GFP and were immunoblotted with the antibodies indicated. (*B*) The binding of PBD to CAP-D3 is lost in the T1415A mutant. The indicated series of GFP-tagged CAP-D3 proteins were immunoprecipitated (*top* panel) and analyzed by Far-Western analysis with PBD (*bottom* panel). Note that, like the endogenous protein, GFP-CAP-D3 can be detected as two major bands in mitotic extracts from the wild-type and S729A and S1329A mutant cells, but not the T1415A cells. (*C*) A PBD-binding motif in CAP-D3. Among three candidate sites, Thr 1415 and Ser 1419 fall within a PBD-binding motif (boxed) and the Plk1 consensus phosphorylation site (color-coded), respectively. Equivalent regions from orthologous proteins from different species are aligned, highlighting the evolutionary conservation of these motifs. The numbers in brackets indicate positions of the Thr 1415-equivalent threonine (bold) in the full amino acid length of CAP-D3 protein. (*D*) Cdk1 and Plk1 mediate phosphorylation of Thr 1415 and Ser 1419, respectively, in vitro. A series of polypeptides corresponding to a partial fragment of CAP-D3 that encompasses the prospective phosphorylation sites were incubated with mock (control), Cdk1/Cyclin B, or Plk1. (*Top* panels) Incorporation of ^{32}P was detected by autoradiography. (*Bottom* panels) Coomassie Brilliant Blue staining (CBB) verifies that equivalent amounts of substrate appear in each lane.

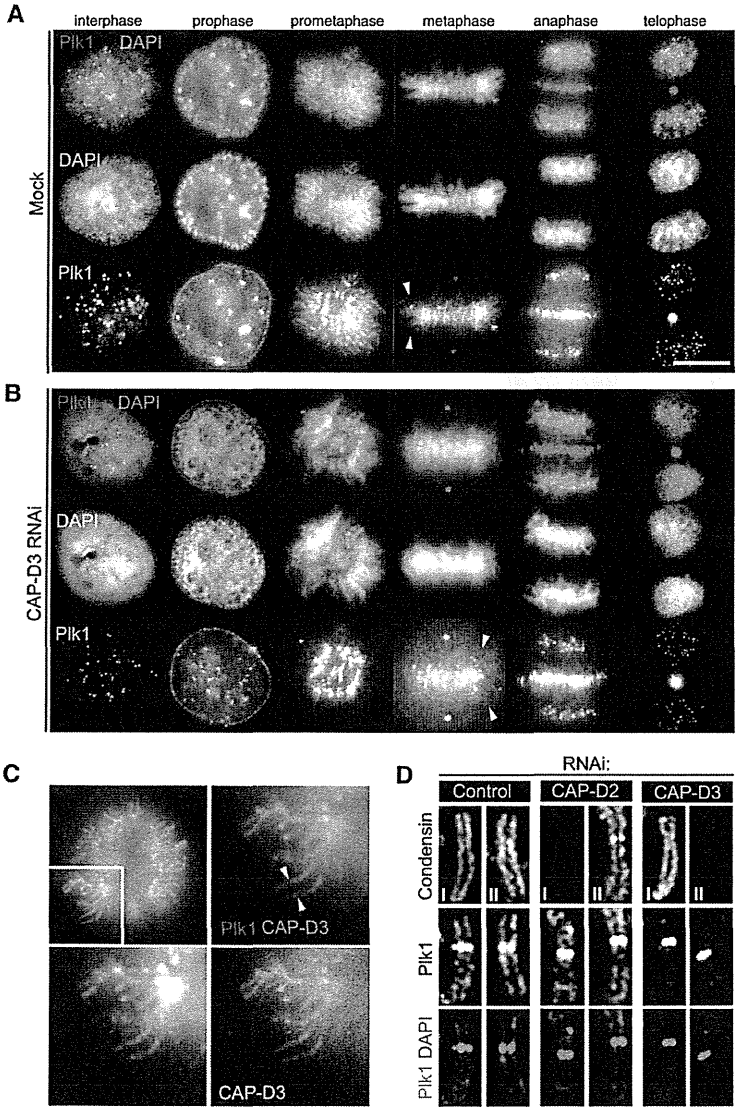

Figure 3. Enrichment of Plk1 on chromosomal axes. (*A*) Localization of Plk1 by immunofluorescence microscopy. Exponentially growing HeLa cells were fixed with methanol, incubated with antibodies to Plk1, and labeled with an Alexa fluorescent dye (red). DNA was stained with DAPI (green). Representative cells in interphase, prophase, prometaphase, metaphase, anaphase, and telophase are shown. Note the chromosome axial staining with Plk1 antibodies in prometaphase and metaphase (arrowheads). Bar, 10 μm. (*B*) Enrichment of Plk1 on chromosome axes is lost in the absence of CAP-D3. Cells depleted of CAP-D3 were processed for immunofluorescence microscopy as in *A*. Note that Plk1 signals on chromosome axes are displaced (arrowheads), while the other localizations are preserved. (*C*) Colocalization of Plk1 with CAP-D3. Wild-type GFP-CAP-D3-expressing cells were fixed and stained with Plk1 antibodies. Both CAP-D3 (*right bottom* panel; green in *top* merged panels) and Plk1 (*left bottom* panel; red in *top* merged panels) signals are visible on chromosome axes. (*D*) Enrichment of Plk1 at chromosome axes depends on condensin II but not condensin I. Chromosome spread samples prepared from mitotic cells that had been depleted of CAP-D2, CAP-D3, or mock (control) were fixed and stained for Plk1 with either condensin I (CAP-H) or condensin II (CAP-D3), as indicated. Quantification of fluorescence intensities for Plk1 signals is shown in Supplemental Figure 5A.

seen and abolished in CAP-D3-depleted cells but not in cells depleted of a condensin I subunit, CAP-D2 (Fig. 3D).

To address whether this CAP-D3-dependent chromosomal axis localization of Plk1 requires phosphorylation at Thr 1415, as the above biochemical assays suggested (Fig. 2), we generated a series of cell lines that stably express GFP-tagged nonphosphorylatable alanine mutants, and depleted endogenous CAP-D3 proteins from those cells. The immunoblot analysis of cell extracts showed that the endogenous protein was largely replaced with GFP-tagged CAP-D3 for each cell line (Fig. 4A). Under these conditions, we found that the chromosomal axis-enriched Plk1 became undetectable in T1415A-replaced cells, whereas wild-type-replaced or S1419A-replaced cells retained the axial Plk1 staining (Fig. 4B, arrowheads). These findings were further confirmed by immunofluoresence microscopy of spread chromosomes (Fig. 4C).

Regulation of CAP-D3 phosphorylation in vivo

Thus, the recruitment of Plk1 to chromosomal axes depends on the binding to CAP-D3, and crucial to this is the phosphorylation of this subunit on the Thr 1415 residue. To elucidate the regulation of CAP-D3 phosphorylation in vivo, we generated antibodies named pT1415 and pS1419, which can primarily recognize CAP-D3 when Thr 1415 or Ser 1419 residues are phosphorylated, respectively. Using these antibodies for immunoblot analyses, we found two phosphorylated species of CAP-D3 in mitotic cell extract; phosphorylation at Thr 1415 is seen in both bands, whereas phosphorylation at Ser 1419 contributes only in the upper band; i.e., the hyperphosphorylated form (Fig. 4D). As generation of the hyperphosphorylated form of CAP-D3 depends on the Plk1 activity (Fig. 1D), this finding implies that Ser 1419 is a phospho-site of Plk1.

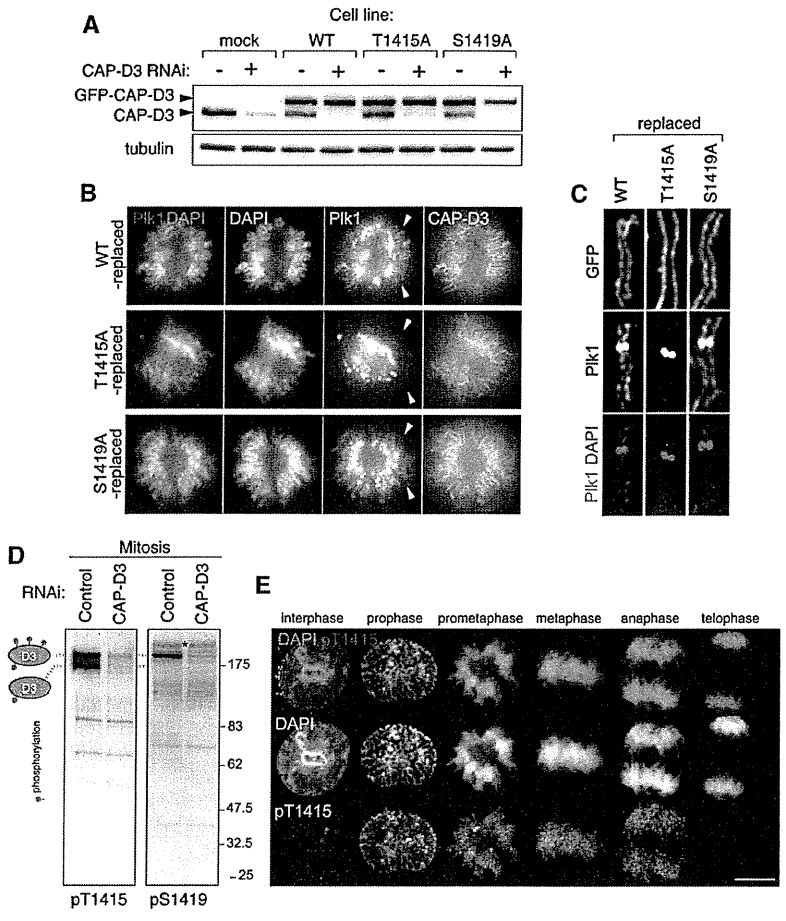

Figure 4. Mitotic phosphorylation of CAP-D3 on Thr 1415 and Ser 1419. (*A*) Replacement of endogenous CAP-D3 protein with GFP-tagged CAP-D3 proteins. HeLa cells that stably express GFP-tagged GFP-D3, either wild-type (WT) or the nonphosphorylatable mutant for Thr 1415 (T1415A) or Ser 1419 (S1419A), were generated. Expression of endogenous CAP-D3 was suppressed by RNAi designed to target the untranslated region of the gene. Interphase cell extracts were analyzed by immunoblotting for the amount of endogenous CAP-D3 (*bottom* bands) and GFP-CAP-D3 (*top* bands). (*B*) Delocalization of Plk1 from chromosome axes in T1415A-replaced cells. Wild-type-replaced, T1415A-replaced, or S1419A-replaced cells were fixed and stained with Plk1 antibodies (red). DNA was stained with DAPI (green). Representative prometaphase cells are shown. Note that T1415A and S1419A were both found enriched at chromosomal axes at levels comparable with the wild-type version, which discounts the possibility that these phosphorylations have a major role in the chromosomal association of condensin II. (*C*) Enrichment of Plk1 at chromosome axes is perturbed in T1415A-replaced cells. Fixed chromosome spread samples prepared from mitotic cells that had been replaced with the indicated version of CAP-D3 were stained with Plk1 antibodies. Quantification of fluorescence intensities for Plk1 signals is shown in Supplemental Figure 5B. (*D*) Generation of phospho-specific CAP-D3 antibodies. Total extracts of nocodazole-arrested cells treated with either mock (control) or CAP-D3 RNAi were subjected to immunoblotting by pT1415 or pS1419 antibodies. Note that two major pT1415 reactive bands and one major pS1419 reactive band (as denoted on the *left* side) are diminished in CAP-D3-depleted cells. Bands that do not disappear after CAP-D3 depletion are nonspecific reactive proteins (a band marked by an asterisk, for example). Specific reactivity to phospho-sites and mitotic forms are later shown in Supplemental Figure 6, A and B, respectively. (*E*) Timing of CAP-D3 Thr 1415 phosphorylation during mitotic progression. Fixed HeLa cells were stained with pT1415 antibodies and labeled with an Alexa dye (red). DNA was stained with DAPI (green). Representative pictures of interphase, prophase, prometaphase, metaphase, and early and late anaphases are shown. Bar, 10 μm. For pl419 staining, see Supplemental Figure 6B.

Immunofluoresence microscopy using pT1415 and pS1419 demonstrated that these modifications take place specifically in mitosis, from prophase to early anaphase (Fig. 4E; Supplemental Fig. 6B). The finding that phosphorylation of Thr 1415 induces Plk1 to bind CAP-D3 raises the possibility that phosphorylation of Ser 1419 is facilitated by CAP-D3-bound Plk1. In line with this idea, we noticed that the chromosome staining with pS1419 antibodies is diminished in T1415A-replaced cells (Fig. 5A). Immunoblotting analysis also suggested that the levels of Ser 1419 phosphorylation were reduced without Thr 1415 phosphorylation (Fig. 5B, lane 14; Supplemental Fig. 6B, lane 8). These data support the notion that phosphorylation of Ser 1419 is efficiently catalyzed by CAP-D3-bound Plk1. In this experiment, we also noticed that the hyperphosphorylation of CAP-D3 is suppressed in T1415A-replaced cells (Fig. 5B, lane 4; Supplemental Fig. 6B, lane 2), suggesting that phosphorylation of Thr 1415 is required for hyperphosphorylation of CAP-D3. Moreover, the finding that S1419A has little effect on hyperphosphorylation of CAP-D3 implies the existence of other Plk1-mediated phospho-sites (Fig. 5B, lane 5).

Phosphorylation of CAP-D3 Thr 1415 triggers full phosphorylation of condensin II

As the other condensin II subunits, CAP-G2 and CAP-H2, undergo Plk1-dependent phosphorylation (Fig. 1D), we asked whether phosphorylation of these subunits also relies on Thr 1415 phosphorylation (Fig. 6A). In mitotic extracts, CAP-G2 can be detected as two major bands, the upper being the hyperphosphorylated form (Figs. 1D, 6A [cf. lanes 1 and 2]). We found that the upper band was decreased in T1415A-replaced cells (Fig. 6A, lane 8), as in

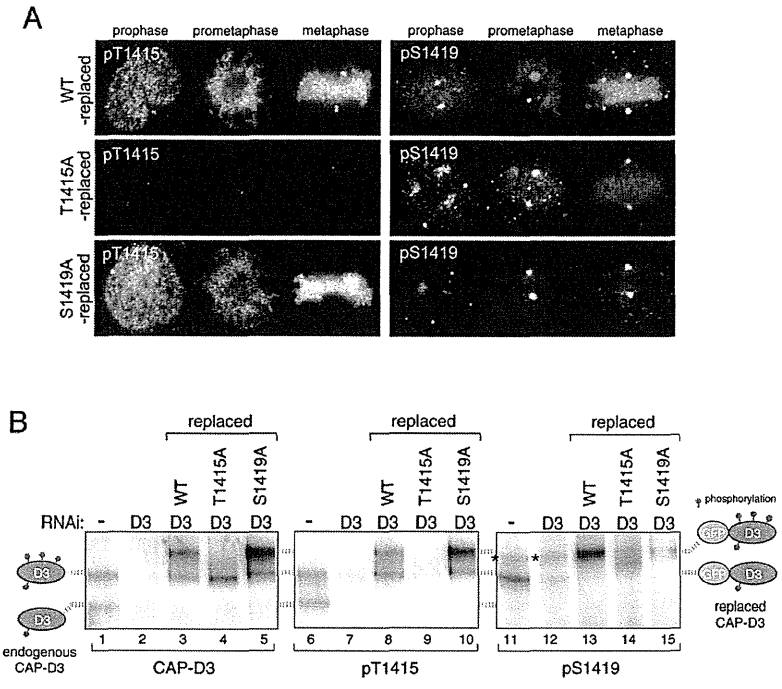

Figure 5. Hyperphosphorylation of CAP-D3 depends on CAP-D3-bound Plk1. (*A*) Reduced levels of Ser 1419 phosphorylation in T1415A-replaced cells. Cells in which endogenous CAP-D3 was replaced by either wild-type (*top* panels), T1415A (*middle* panels), or S1419A (*bottom* panels) forms of GFP-CAP-D3 were fixed and stained with pT1415 or pS1419 antibodies. Note that pS1419 antibodies cross-react with an unidentified epitope at centrosomes, seen as two marked dots that do not disappear after depletion of CAP-D3. Quantification of fluorescence intensities is summarized in Supplemental Figure 5, C and D. (*B*) Regulation of Thr 1415 and Ser 1419 phosphorylation. (First two lanes of each panel) Two species with different phosphorylation levels of endogenous CAP-D3 can be detected in mitotic cell extracts that diminish after CAP-D3 depletion, as depicted on the *left* side. (Last three lanes of each panel) Mitotic extracts from wild-type-replaced, T1415A-replaced or S1419A-replaced cells were analyzed. As replaced CAP-D3 proteins are tagged with GFP, they migrate slower than the endogenous proteins. The two corresponding phosphorylated forms of GFP-CAP-D3 are positioned on the *right* side. Asterisks mark nonspecific bands, which do not appear in immunopurified GFP-CAP-D3 samples (Supplemental Fig. 6A).

cells depleted of CAP-D3 or Plk1 (Fig. 6A, lanes 3,4). Likewise, the mitotic mobility retardation of CAP-H2 was mostly abolished in these three conditions (Fig. 6A, lanes 3,4,8). These results suggest that Plk1 bound to CAP-D3 facilitates hyperphosphorylation of all of the non-Smc subunits of condensin II. Of note, threonine residues in the C-terminal region of condensin I subunit CAP-D2 have been identified as a mitotic phosphorylation target of Cdk1 in frog extracts (Kimura et al. 1998). However, CAP-D2 does not seem to participate in recruiting Plk1, as depletion of CAP-D2 did not displace Plk1 from chromosomal axes (Fig. 3D).

Having been able to detect phosphorylations on CAP-D3 in vivo, we wished to identify the kinases involved. A 20-min pretreatment of mitotic cells with a Cdk1 inhibitor abolished phosphorylation of Thr 1415, and pretreatment with a Plk1 inhibitor reversed Ser 1419 phosphorylation (Fig. 6B). Together with in vitro experiments (Fig. 2), these results suggest that phosphorylation of Thr 1415 and Ser 1419 depends primarily on Cdk1 and Plk1, respectively. The Ser 1419 phosphorylation was also reversed by inhibiting Cdk1 (Fig. 6B), consistent with the idea that phosphorylation of Thr 1415 is a crucial step to induce further Plk1-mediated phosphorylation of condensin II. Based on these observations, we propose that the Cdk1-mediated phosphorylation of CAP-D3 Thr 1415 creates a binding module for the PBD, and CAP-D3-bound Plk1 further promotes hyperphosphorylation of the whole condensin II complex, including CAP-D3 itself (Fig. 6C).

Phosphorylation stimulates the activity of condensin II

Finally, to investigate the consequences of condensin II phosphorylation, we carried out live-cell imaging analysis and monitored the behavior of chromosomes during mitotic progression (Fig. 7A,B). Similar to previous studies (Hirota et al. 2004; Ono et al. 2004), the initial phase of chromosome condensation typically became discernible ~15 min before NEBD and progressed during prophase. In CAP-D3-depleted cells, the condensation was delayed and appeared only a few minutes before NEBD. This defective chromosome condensation in prophase after CAP-D3 depletion was recovered by expressing wild-type CAP-D3. In contrast, the T1415A mutant failed to rescue the defect; cells largely lacked chromosome condensation during prophase, when it arose shortly before NEBD, as seen in CAP-D3-depleted cells.

To supplement these observations in live cells, we additionally assessed the extent of chromosome condensation in fixed-cell preparations. As shown previously (Hirota et al. 2004), inactivation of condensin II by CAP-D3 depletion caused a strong reduction in chromosome condensation in prophase. This reduction was sufficiently recovered by expressing either wild-type CAP-D3 or the S1419A mutant, but not the T1415A mutant (Supplemental Fig. 7). These experiments indicate that CAP-D3 phosphorylation at Thr 1415 is a key modification for condensin II to initiate chromosome condensation in prophase.

One chromosome morphology related to condensin II depletion is known as "curly" chromosomes (Ono et al.

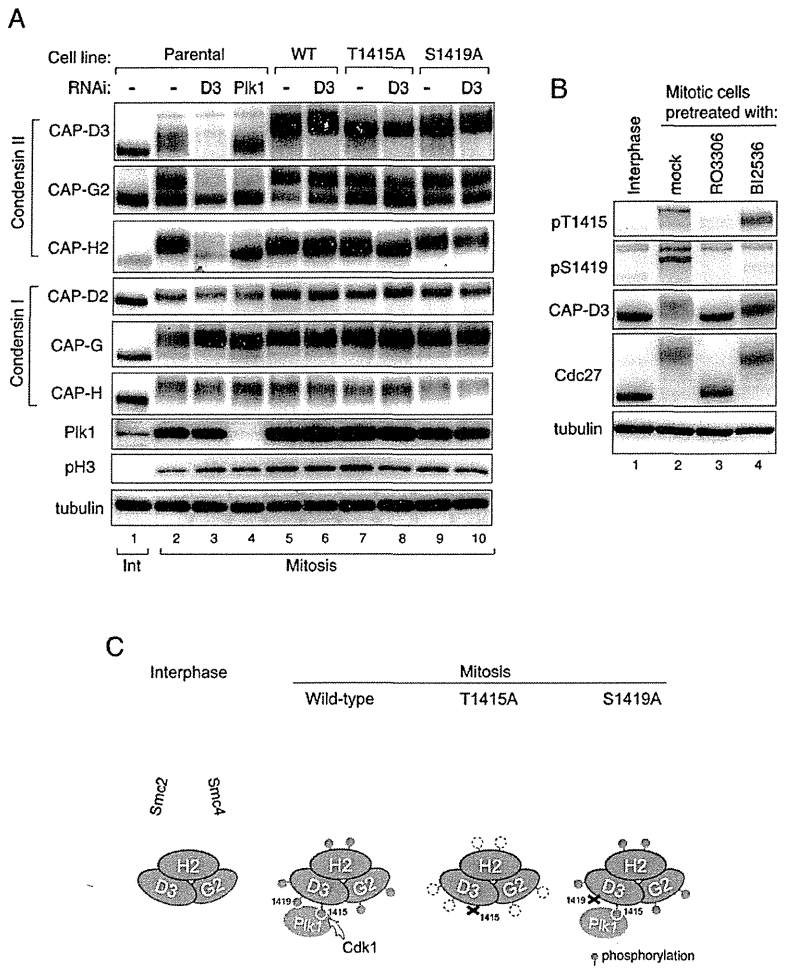

Figure 6. Cdk1-mediated phosphorylation of Thr 1415 is required for the full phosphorylation of condensin II. (*A*) Mitotic phosphorylation of non-Smc subunits of condensin II is perturbed in the T1415A mutant. Mitotic cell extracts prepared from indicated cell lines, with or without RNAi to Plk1 or to CAP-D3, were analyzed with the antibodies to condensin subunits. Parental cell line indicates the cell population that does not express any tagged protein. Note that changes in phosphorylation levels, as seen for condensin II subunits, are not readily detectable for condensin I subunits. (*B*) Phosphorylation of Thr 1415 and Ser 1419 depends primarily on Cdk1 and Plk1, respectively. Total cell extracts were prepared from thymidine-arrested interphase cells (lane *1*) or nocodazole-arrested mitotic cells (lanes *2–4*) in which the activity of Cdk1 or Plk1 is inhibited by RO3306 or BI2536 treatment, respectively (lanes *3,4*), and were analyzed by immunoblotting using the antibodies indicated. Note that pT1415 and pS1419 antibodies can hardly detect CAP-D3 protein in interphase cells (cf. lanes *1* and *2*), indicating the specific reactivity of these antibodies to mitotic phosphorylated forms. (*C*) Illustrations depicting how condensin II complex is phosphorylated in mitosis, and how phosphorylations are affected in the T1415A and S1419A mutants. The model predicts the crucial role of Cdk1 in phosphorylating CAP-D3 at Thr 1415, which triggers the full phosphorylation of the condensin II complex, and explains why the phosphorylation levels are markedly decreased in T1415A-replaced but not S1419A-replaced cells.

2003). This characteristic structural change, emerging after treating cells with a hypotonic condition, is thought to reflect an improper chromosome assembly in the absence of condensin II. We found that 50% of the T1415A-replaced cells had chromosomes with the typical curly change, whereas in control wild-type-replaced cells, only 15% were affected. Importantly, 27% of the S1419A-replaced cells were found to have curly chromosomes, which implies that the Plk1-mediated phosphorylation of CAP-D3 is directly involved in mitotic chromosome assembly (Fig. 7D,E). Concomitantly, we found that T1415A-replaced cells were more susceptible to chromosome segregation failure than controls, as revealed by increased incidence of bridging or lagging chromosomes (Fig. 7C; Ono et al. 2004; Gerlich et al. 2006). The increased frequency of these errors was also seen in S1419A-replaced cells (Fig. 7C).

These results are consistent with the notion that phosphorylation of Thr 1415 and subsequent Plk1-mediated phosphorylation of CAP-D3 are essential for condensin II's function to properly assemble chromosomes and prevent segregation errors. Unlike T1415A-replaced cells, however, S1419A-replaced cells did not reveal overt defects in chromosome condensation in prophase (Fig. 7A,B; Supplemental Fig. 7). We suspect that this is because defects in chromosome condensation in prophase cells lacking a single Plk1 phosphorylation site were beyond the detection level of the light microscope. As Ser 1419 phosphorylation seems to already appear in prophase (Supplemental Fig. 6B), it is possible that chromosome assembly in prophase involves Plk1-mediated phosphorylation of condensin II.

Discussion

CAP-D3 phosphorylation at Thr 1415 is crucial for condensin II function

Mitotic chromosome assembly in prophase was largely suppressed in Thr 1415 nonphosphorylatable mutant cells, which indicates a key role of CAP-D3 phosphorylation on this particular site for the function of condensin II. In eukaryotic cells whose nuclear envelopes disassemble in mitosis, chromosome condensation seems to

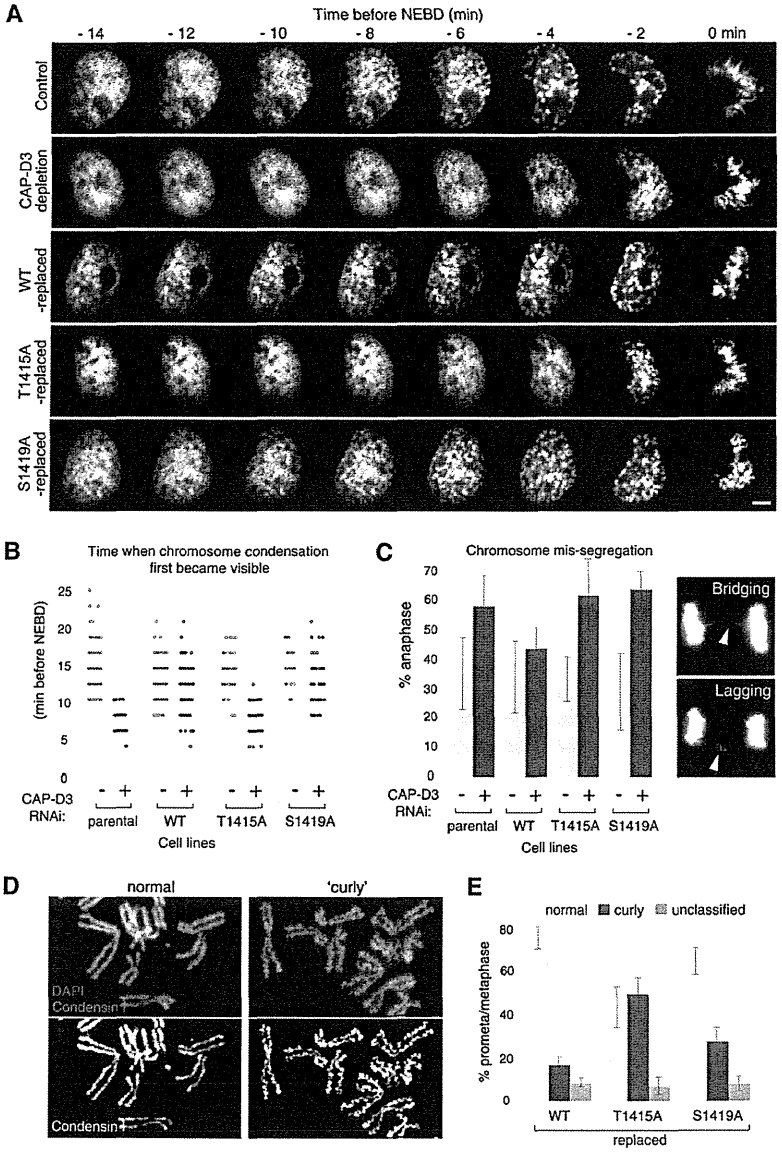

Figure 7. Nonphosphorylatable CAP-D3 mutants defective in mitotic functions of condensin II. (*A*) Analysis of the initial phases of chromosome condensation in live cells. Prophase image sequences were aligned on the time axis according to time before NEBD, which is defined by loss of a defined nuclear boundary. Bar, 5 μm. (*B*) Quantification of chromosome condensation in prophase. Time (minutes before NEBD) when chromosome condensation first became recognizable was scored and plotted for the indicated live-cell recordings. (*C*) Analysis of defective chromosome segregation in anaphase in nonphosphorylatable CAP-D3 mutants. During live-cell imaging analysis, anaphase cells were assessed for the presence of lagging and/or bridging chromosomes, as exemplified in the panels on the *right*. Mean ± SD from three experiment replicates (n = 20~30 cells per experiment) are shown in the histogram. Similar results were obtained in a fixed-cell analysis (Supplemental Fig. 8). (*D*) Examples of chromosome spreads demonstrating normal (*left* panels) or curly (*right* panels) appearance. Chromosome spreads were prepared from cells that had been treated with a hypotonic buffer and stained with CAP-H (a condensin I subunit) antibodies (red). DNA was counterstained with DAPI (green). (*E*) Abnormal curly change of chromosomal axes in nonphosphorylatable CAP-D3 mutants. More than 100 cells per indicated condition were examined and scored based on their chromosomal axis appearance (mean ± SD).

initiate universally in prophase; i.e., before the NEBD. Our amino acid sequence conservation analysis identified a PBD-binding motif in conjunction with an adjacent prospective phospho-site in the C-terminal region of CAP-D3 protein in mammals as well as in worms and flies (Fig. 2C), but not in the budding/fission yeast CAP-D3 counterparts Ycs4/Cnd1. An attractive hypothesis would be, therefore, that CAP-D3 phosphorylation at Thr 1415 or the equivalent site plays an essential role in activating condensin II, and thereby triggers chromosome condensation in prophase in all eukaryotes undergoing open mitosis.

In addition to the defective chromosome condensation in prophase, we found that chromosomes in the Thr 1415 mutant cells often reveal a curly appearance of chromosomal axes and an increasing rate of chromosome segregation failure (Fig. 7). Taking into account a FRAP experiment that indicated that condensin II complexes bind stably to chromosomes throughout mitosis (Gerlich et al. 2006), condensin II complexes bearing the T1415A mutant possibly stay on chromosomes throughout mitosis once they are loaded during prophase. If so, we consider it plausible that the chromosomal phenotypes after NEBD are causally related to condensin II's inability to induce chromosome condensation in prophase.

How does phosphorylation regulate condensin II?

How might phosphorylation at Thr 1415 mechanistically stimulate the activity of condensin II? The mass

spectrometric analysis pointed out multiple phosphosites on CAP-D3, and thus Thr 1415 would not be the only residue that is phosphorylated by Cdk1; still, our findings identify it as a key site that promotes further phosphorylation of the condensin II complex by Plk1. The Polo kinase-mediated phosphorylation of condensin has been shown to stimulate its supercoiling activity in budding yeast (St-Pierre et al. 2009). Thus, there is a precedent for the regulation of condensin via Plk1-mediated phosphorylation, and this mechanism may be conserved through evolution for the regulation of condensin II. Supporting this possibility, the S1419A mutation perturbed the ability of condensin II to induce mitotic chromosome assembly properly (Fig. 7C–E; Supplemental Fig. 8).

It is important to point out, however, that identification of Plk1 as a kinase for condensin II does not discount the possibility that phosphorylation by Cdk1 per se contributes to the activation of condensin II, as was originally proposed for condensin I (Kimura et al. 1998). The fact that chromosome condensation takes place before the NEBD in cells depleted of Plk1 activity (Lenart et al. 2007) allows us to hypothesize that phosphorylation of Cdk1 itself can stimulate the activity of condensin II, at least to some extent. Consistent with this view, in yeast, phosphorylation by Cdk1 alone can partially stimulate the ability of condensin to induce supercoils (St-Pierre et al. 2009).

Analogous to condensin I, phosphorylation of condensin II might mediate the chromosomal localization of condensin II. However, we noticed that the nonphosphorylatable CAP-D3 mutants T1415A and S1419A were both found enriched at chromosome axes at levels comparable with the wild-type version (Fig. 4B), precluding the possibility that these phosphorylations by Cdk1 and Plk1 have a major role in the chromosomal association of condensin II. This interpretation is also consistent with the recent finding that chromosomal targeting of condensin II is mediated through the action of PP2A (Takemoto et al. 2009). Thus, instead of controlling the localization, we propose that the phosphorylation stimulates the activity of condensin II to promote mitotic chromosome assembly.

Enrichment of Plk1 at chromosome axes

A prominent feature of Plk1 is that this kinase changes its localization to various cellular structures during mitotic progression (including centrosomes, kinetochores, and the central spindle), which appears to be important to conduct specific functions at the right place (for review, see Petronczki et al. 2008; Archambault and Glover 2009). Our data are consistent with the model that Plk1 is recruited to chromosome axes along chromosome arms by binding to CAP-D3, and that CAP-D3-bound Plk1 further mediates phosphorylation of condensin II subunits. An obvious follow-up question is to ask whether the range of Plk1 activities is confined to the condensin II complex, or whether it can also promote phosphorylation of other chromosomal proteins. Surprisingly, when electrophoretic mobility retardation is used as a readout for protein phosphorylation, Plk1 does not seem to act on the closely related complex condensin I (Fig. 1D), which also localizes at chromosome axes, but this might simply be because condensin I is not a substrate for Plk1.

It would be interesting to find out next whether topoisomerase IIα is controlled by the chromosomal axis-enriched Plk1, as this enzyme becomes enriched at chromosome axes in prophase to promote chromosome assembly (Gimenez-Abian et al. 1995) and is found to undergo Plk1-dependent mitotic phosphorylation (Santamaria et al. 2011). However, we speculate that the function of topoisomerase IIα to shorten chromatid lengths is not directly regulated by Plk1 on axes because we have never seen that condensin II depletion, a condition that displaces Plk1 from chromosome axis, resulted in abnormally long chromosomes (Hirota et al. 2004). These observations support the view that Plk1 has a very special mode of action in that it requires physical binding to its substrates to ensure efficient phosphorylation, and therefore the activity of the kinase can, in principle, reach to its bound protein or the protein complex to which Plk1 is bound. Such confined action of Plk1 contrasts with the properties of other mitotic kinases.

Plk1 has been implicated in the phosphorylation of the cohesin complex during the so-called "prophase pathway," the mechanism that removes cohesin complexes from chromosome arms in prophase (Losada et al. 2002; Sumara et al. 2002). An interesting question to ask is whether cohesin complexes enriched in between sister chromatids are targeted by CAP-D3-bound Plk1. However, the prophase pathway seems to be intact in cases in which Plk1 had been depleted or displaced from chromosome axes, because both dissociations of sister chromatid cohesion between chromosome arms seem to proceed normally under those conditions (Supplemental Fig. 9). How might Plk1 then act on cohesin on chromosome arms? Having found the confined action of Plk1 to condensin II, we consider it possible that Cdk1 phosphorylates one of the cohesin subunits and recruits Plk1, which enables an efficient phosphorylation of the cohesin complex. This hypothesis would provide an intriguing view of how Cdk1 activity promotes dissociation of sister chromatid cohesion on the chromosome arms, which proceeds in parallel to chromosome condensation in cells entering mitosis.

Materials and methods

Antibodies

Polyclonal rabbit antibodies to condensin complexes were raised by immunizing two peptides in combination for each subunit, as follows: CAP-D3 (CTKRAISTPEKSISD [corresponding amino acid sequence number 1409–1422] and CSRRSLRKTPLKTAN [1484–1498]), CAP-D2 (EFHLPLSPEELLKSC [7–20] and CTTPIL RASARRHR [1388–1400]), CAP-H2 (CRTNVDLKNDQTPSE [78–91] and CKRFQTYAAPSMAQP [543–556]), CAP-G2 (CGED NMETEHGSKMR [77–90] and CYESSSRTLGELLNS [1130–1143]), Smc4 (AGEKILGPFHKRFSC [10–24] and VAVNPKEIAS KGLC [1189–1202]). The resulting antisera were affinity-purified

against the peptides used for immunization. Antibodies to Smc2 and CAP-H were generously provided by Jan-Michael Peters (Research Institute of Molecular Pathology, Vienna), and CAP-G is published in Nakajima et al. (2007) . The phospho-specific antibodies pT1415 and pS1419 were raised against synthetic phospho-peptides CTKRAIS(pT)PEKSISDVTF and CTPEK(pS)ISDVT, respectively, in rabbits. The resulting antisera were subjected to sequential affinity purification on phospho-peptide and non-phospho-peptide columns. The following monoclonal mouse antibodies were used: Plk1 (F8, Santa Cruz Biotechnology), Cyclin B1 (clone 18, BD Biosciences), α-tubulin (B512, Sigma), GFP (G1544, Sigma), Cdc27 (clone 35, BD Biosciences).

Immunoblot and Far-Western analyses

Cells were extracted in a buffer consisting of 20 mM Tris-HCl (pH 7.4), 100 mM NaCl, 20 mM β-glycerophosphate, 5 mM $MgCl_2$, 0.1% Triton X-100, 10% glycerol, and 1 mM DTT, supplemented with a cocktail of protease inhibitors (Complete Mini EDTA-free, Roche Diagnostics). When looking for electrophoretic mobility shifts, extraction was performed in the presence of 100 nM okadaic acid, 2 mM Na_3VO_4, and 10 mM NaF. To control the protein amount loaded per lane, total protein concentration of cell lysates was measured by the Bradford method (Protein Assay System, Bio-Rad Laboratories). Immunoblotting was performed as described previously (Nakajima et al. 2007). The recombinant PBD protein was purified from bacteria expressing a GST-fused C-terminal fragment of Plk1 (spanning amino acid residues 305–903) that contains the PBD. Far-Western assays were performed with the recombinant GST-PBD protein (20 μg/mL) in Tris-buffered saline (TBS) containing 1% skim milk and 0.01% Triton X-100 for 3 h at 4°C, followed by detection of bound proteins with monoclonal Plk1 antibodies that recognize its C-terminal fragment.

Immunoprecipitation

Mitotic cells were lysed in immunoprecipitation buffer (20mM Tris-HCl at pH 7.5, 150 mM NaCl, 20 mM β-glycerophosphate, 5 mM $MgCl_2$, 0.1% NP-40, protease inhibitors [Complete Mini EDTA-free, Roche], 1 mM DTT), supplemented with 100 nM okadaic acid, 2 mM Na_3VO_4, 10 mM NaF, and 0.25 U/L benzonase nuclease (Novagen), for 20 min on ice. Cell extracts, after removing the insoluble fraction by centrifugation at 15,000 rpm for 30 min at 4°C, were used for immunoprecipitation. Typically, 10 μL of protein A (Bio-Rad) or protein G-Sepharose (GE Healthcare) beads coupled to antibodies were incubated with cell extracts for 2 h at 4°C, then washed three times with immunoprecipitation buffer and three times with 0.05% TBS-Tween20. Mass spectrometry was performed as described (Nozawa et al. 2010). Dephosphorylation of immunoprecipitated condensin was performed on beads using λ-phosphatase (New England Biolabs) in a buffer containing 50 mM Tris-HCl (pH 7.5), 0.1 mM Na_2EDTA, 5 mM DTT, and 2 mM $MnCl_2$ for 30 min at 30°C.

Cell synchronization, inhibitor treatment, and cell lines

HeLa cells were cultured and synchronized with a double-thymidine block protocol as described previously (Nakajima et al. 2007). Mitotic cells were shaken off and collected from cell culture dishes that had been treated for 3 h with 50 ng/mL nocodazole, which was added at a 6 h-time point after the release from the second thymidine block. These mitotic cells were then treated with 10 μM RO3306 (Roche) or with an equivalent concentration of the solvent DMSO (mock) for 20 min before being harvested for immunoblot analyses. To inhibit Plk1 activity, 100 nM BI2536 (Tocris) was added at the 6-h time point with nocodazole. To generate cell lines that stably express fluorescent-tagged proteins, plasmids encoding a series of AcGFP-CAP-D3 were transfected using FuGENE 6 reagent (Roche). Stably expressing cell clones were selected in a complete medium containing 0.2 μg/mL puromycin and verified by fluorescence microscopy and immunoblotting for the expression of the tagged transgene.

RNAi

The sequences of the siRNAs were as follows: CAP-D3, 5′-AGG AAUUCAAGUUAACAGAGGCUUG-3′; Plk1, 5′-CGCCCAAC CAUUAACGAGCUGCUUA-3′. The cells were transfected by incubating 50 nM duplex siRNA with RNAi-MAX transfection reagent (Invitrogen) in antibiotic-free growth medium. RNAi treatment was performed concomitantly with the synchronization with thymidine; the length of substantial transfections with siRNA targeting CAP-D3 and Plk1 was 48 h and 24 h, respectively. For control transfections, the same annealing reaction was set up using H_2O instead of siRNA oligonucleotides.

In vitro phosphorylation

Recombinant GST-fused CAP-D3 fragments (amino acid sequence 1399–1429), including wild-type and mutants, were expressed in bacteria BL21 and purified using glutathione beads, and used as kinase substrates. Reactions were carried out for 30 min at 37°C in a kinase reaction buffer (5 mM MOPS at pH 7.2, 2.5 mM β-glycerolphosphate, 5 mM $MgCl_2$, 1 mM EGTA, 0.4 mM EDTA, 100 ng/μL BSA, 10 mM DTT, 1 mM ATP, 1 μCi/μL [γ-^{32}P]ATP). The protein kinases used were recombinant Cdk1/Cyclin B (Carna Bioscience) or Plk1 (Cell Signaling Technology). Phosphorylation of GST-fused CAP-D3 fragments was detected by autoradiography.

Immunofluorescence microscopy

Cells grown on coverslips were fixed with ice-chilled 100% methanol for 20 min at −20°C, or with 2% paraformaldehyde in 0.137 M sodium phosphate buffer (pH 7.4). In some cases, a pre-extraction protocol was carried out for 2 min in 0.1% Triton X-100–PBS, followed by a 3-min incubation in PBS before fixation. Fixed cells were permeabilized with 0.2% Triton X-100–PBS and incubated with 3% BSA/PBS for at least 1 h. In some experiments, mitotic cells were shaken off, immersed in a hypotonic buffer (PBS:distilled water = 2:3 solution) for 5 min, and spun onto glass slides at 1000 rpm for 5 min using a cytospin centrifuge (Shandon). Cells were incubated with the primary antibodies overnight at room temperature, followed by incubation with secondary antibodies for 1 h. The secondary antibodies used in this study were goat anti-rabbit IgG Alexa fluor 488 and 568, goat anti-mouse Alexa fluor 488 and 568, and goat anti-human IgG Alexa fluor 568 (Molecular Probes). After a 5-min incubation with 0.1 μg/mL 4′,6-diamidino-2-phenylindole (DAPI), cells were mounted in Prolong Gold anti-fade mounting reagent (Invitrogen). Images were acquired on a Zeiss Imager Z.1 microscope equipped with epifluorescence and a Photometrics Cool Snap HQ CCD camera.

Live-cell imaging analysis

Cells were placed into CO_2-independent medium without phenol red (Gibco) on Lab-Tek chambered coverslips (Nunc), and the chamber lids were sealed with silicone grease. Images were captured every 2 min, with 100-msec exposure times, through a 100×/1.40 NA Plan Apochromat oil objective lens mounted on

an inverted microscope (IX-71; Olympus) equipped with a Cool Snap HQ CCD camera (Photometrics). A series of projected images of five *Z*-sections with 4.0-μm intervals were analyzed.

Acknowledgments

We are grateful to Keiji Kimura (Tsukuba University) for CAP-D3 cDNA, Jan-Michael Peters (IMP, Vienna) for CAP-H and Smc2 antibodies, Kazuki Kumada (JFCR Cancer Institute, Tokyo), and James Hutchins (IMP, Vienna) for crucial comments on the manuscript. Research in the laboratory of T.H. is supported by grants from the Japan Society for the Promotion of Science (JSPS) and the Ministry of Education, Culture, Sports and Technology of Japan (MEXT), and a research grant from the Cell Science Research Foundation.

References

Archambault V, Glover DM. 2009. Polo-like kinases: conservation and divergence in their functions and regulation. *Nat Rev Mol Cell Biol* **10:** 265–275.

Elia AE, Rellos P, Haire LF, Chao JW, Ivins FJ, Hoepker K, Mohammad D, Cantley LC, Smerdon SJ, Yaffe MB. 2003. The molecular basis for phosphodependent substrate targeting and regulation of Plks by the Polo-box domain. *Cell* **115:** 83–95.

Gerlich D, Hirota T, Koch B, Peters JM, Ellenberg J. 2006. Condensin I stabilizes chromosomes mechanically through a dynamic interaction in live cells. *Curr Biol* **16:** 333–344.

Giet R, Glover DM. 2001. *Drosophila* aurora B kinase is required for histone H3 phosphorylation and condensin recruitment during chromosome condensation and to organize the central spindle during cytokinesis. *J Cell Biol* **152:** 669–682.

Gimenez-Abian JF, Clarke DJ, Mullinger AM, Downes CS, Johnson RT. 1995. A postprophase topoisomerase II-dependent chromatid core separation step in the formation of metaphase chromosomes. *J Cell Biol* **131:** 7–17.

Hagstrom KA, Holmes VF, Cozzarelli NR, Meyer BJ. 2002. *C. elegans* condensin promotes mitotic chromosome architecture, centromere organization, and sister chromatid segregation during mitosis and meiosis. *Genes & Dev* **16:** 729–742.

Hirano T. 2005. SMC proteins and chromosome mechanics: from bacteria to humans. *Philos Trans R Soc Lond B Biol Sci* **360:** 507–514.

Hirano T. 2009. Let's play polo in the field of condensation. *Mol Cell* **34:** 399–401.

Hirota T, Gerlich D, Koch B, Ellenberg J, Peters JM. 2004. Distinct functions of condensin I and II in mitotic chromosome assembly. *J Cell Sci* **117:** 6435–6445.

Kaitna S, Pasierbek P, Jantsch M, Loidl J, Glotzer M. 2002. The aurora B kinase AIR-2 regulates kinetochores during mitosis and is required for separation of homologous chromosomes during meiosis. *Curr Biol* **12:** 798–812.

Kimura K, Hirano M, Kobayashi R, Hirano T. 1998. Phosphorylation and activation of 13S condensin by Cdc2 in vitro. *Science* **282:** 487–490.

Kraft C, Herzog F, Gieffers C, Mechtler K, Hagting A, Pines J, Peters JM. 2003. Mitotic regulation of the human anaphase-promoting complex by phosphorylation. *EMBO J* **22:** 6598–6609.

Lavoie BD, Hogan E, Koshland D. 2004. In vivo requirements for rDNA chromosome condensation reveal two cell-cycle-regulated pathways for mitotic chromosome folding. *Genes & Dev* **18:** 76–87.

Lenart P, Petronczki M, Steegmaier M, Di Fiore B, Lipp JJ, Hoffmann M, Rettig WJ, Kraut N, Peters JM. 2007. The small-molecule inhibitor BI 2536 reveals novel insights into mitotic roles of polo-like kinase 1. *Curr Biol* **17:** 304–315.

Lipp JJ, Hirota T, Poser I, Peters JM. 2007. Aurora B controls the association of condensin I but not condensin II with mitotic chromosomes. *J Cell Sci* **120:** 1245–1255.

Losada A, Hirano M, Hirano T. 2002. Cohesin release is required for sister chromatid resolution, but not for condensin-mediated compaction, at the onset of mitosis. *Genes & Dev* **16:** 3004–3016.

Nakajima M, Kumada K, Hatakeyama K, Noda T, Peters JM, Hirota T. 2007. The complete removal of cohesin from chromosome arms depends on separase. *J Cell Sci* **120:** 4188–4196.

Nasmyth K, Haering CH. 2005. The structure and function of SMC and kleisin complexes. *Annu Rev Biochem* **74:** 595–648.

Nigg EA. 1995. Cyclin-dependent protein kinases: key regulators of the eukaryotic cell cycle. *Bioessays* **17:** 471–480.

Nozawa RS, Nagao K, Masuda HT, Iwasaki O, Hirota T, Nozaki N, Kimura H, Obuse C. 2010. Human POGZ modulates dissociation of HP1α from mitotic chromosome arms through Aurora B activation. *Nat Cell Biol* **12:** 719–727.

Nurse P. 1990. Universal control mechanism regulating onset of M-phase. *Nature* **344:** 503–508.

Ono T, Losada A, Hirano M, Myers MP, Neuwald AF, Hirano T. 2003. Differential contributions of condensin I and condensin II to mitotic chromosome architecture in vertebrate cells. *Cell* **115:** 109–121.

Ono T, Fang Y, Spector DL, Hirano T. 2004. Spatial and temporal regulation of Condensins I and II in mitotic chromosome assembly in human cells. *Mol Biol Cell* **15:** 3296–3308.

Petersen J, Hagan IM. 2003. *S. pombe* aurora kinase/survivin is required for chromosome condensation and the spindle checkpoint attachment response. *Curr Biol* **13:** 590–597.

Petronczki M, Lenart P, Peters JM. 2008. Polo on the rise-from mitotic entry to cytokinesis with Plk1. *Dev Cell* **14:** 646–659.

Santamaria A, Neef R, Eberspacher U, Eis K, Husemann M, Mumberg D, Prechtl S, Schulze V, Siemeister G, Wortmann L, et al. 2007. Use of the novel Plk1 inhibitor ZK-thiazolidinone to elucidate functions of Plk1 in early and late stages of mitosis. *Mol Biol Cell* **18:** 4024–4036.

Santamaria A, Wang B, Elowe S, Malik R, Zhang F, Bauer M, Schmidt A, Silljé HHW, Körner R, Nigg EA. 2011. The Plk1-dependent phosphoproteome of the early mitotic spindle. *Mol Cell Proteomics* **10:** M110.004457. doi: 10.1074/mcp.M110.004457.

St-Pierre J, Douziech M, Bazile F, Pascariu M, Bonneil E, Sauve V, Ratsima H, D'Amours D. 2009. Polo kinase regulates mitotic chromosome condensation by hyperactivation of condensin DNA supercoiling activity. *Mol Cell* **34:** 416–426.

Sumara I, Vorlaufer E, Stukenberg PT, Kelm O, Redemann N, Nigg EA, Peters JM. 2002. The dissociation of cohesin from chromosomes in prophase is regulated by Polo-like kinase. *Mol Cell* **9:** 515–525.

Takemoto A, Murayama A, Katano M, Urano T, Furukawa K, Yokoyama S, Yanagisawa J, Hanaoka F, Kimura K. 2007. Analysis of the role of Aurora B on the chromosomal targeting of condensin I. *Nucleic Acids Res* **35:** 2403–2412.

Takemoto A, Maeshima K, Ikehara T, Yamaguchi K, Murayama A, Imamura S, Imamoto N, Yokoyama S, Hirano T, Watanabe Y, et al. 2009. The chromosomal association of condensin II is regulated by a noncatalytic function of PP2A. *Nat Struct Mol Biol* **16:** 1302–1308.

Yeong FM, Hombauer H, Wendt KS, Hirota T, Mudrak I, Mechtler K, Loregger T, Marchler-Bauer A, Tanaka K, Peters JM, et al. 2003. Identification of a subunit of a novel Kleisin-β/SMC complex as a potential substrate of protein phosphatase 2A. *Curr Biol* **13:** 2058–2064.

Hepatology Research

Hepatology Research 2011; 41: 118–125 doi: 10.1111/j.1872-034X.2010.00749.x

Original Article

Characterization of elevated alanine aminotransferase levels during pegylated-interferon α-2b plus ribavirin treatment for chronic hepatitis C

Yo-hei Aoki,[1] Shogo Ohkoshi,[1] Satoshi Yamagiwa,[1] Masahiko Yano,[1] Hiromichi Takahashi,[1] Nobuo Waguri,[2] Kentaro Igarashi,[2] Soh-ichi Sugitani,[3] Toru Takahashi,[4] Toru Ishikawa,[5] Tomoteru Kamimura,[5] Hiroto Wakabayashi,[6] Toshiaki Watanabe,[7] Yasunobu Matsuda,[1] Minoru Nomoto[1] and Yutaka Aoyagi[1]

[1]*Gastroenterology and Hepatology, Graduate School of Medical and Dental Sciences Niigata University,* [2]*Niigata Municipal Hospital,* [3]*Tachikawa General Hospital,* [4]*Nagaoka Red Cross Hospital,* [5]*Sai-sei-kai Second Hospital,* [6]*Takeda General Hospital, and* [7]*Watanabe Clinic, Niigata, Japan*

Aim: Elevation of alanine aminotransferase (ALT) levels during pegylated-interferon (peg-IFN) plus ribavirin therapy in patients with chronic hepatitis C [CHC] is a problem that cannot be disregarded. The aim of this study is to assess the frequency and to characterize clinical parameters of this phenomenon.

Methods: Two hundred and thirty-five (235) CHC patients with genotype 1b receiving peg-IFN α-2b plus ribavirin therapy were analyzed. Clinical parameters that may be associated with abnormal ALT values during treatment and therapy outcomes were evaluated statistically. One hundred and sixteen (116) patients treated with peg-IFN α-2a plus ribavirin were also included for partial analysis.

Results: Abnormal ALT values during treatment were observed in 23.0% of patients. It was observed in 14.5% of those with sustained virological response (SVR) and 17.8% of those with relapse, in whom viral clearance was observed during therapy. Multivariate logistic regression analysis revealed that pretreatment ALT values, therapy outcome, and body mass index (BMI) were significant factors related to abnormal ALT values during treatment. Abnormal ALT values during treatment became normal in SVR patients at 6 months after the completion of treatment, but not in NR (non-response) patients. Mean ALT values were significantly higher at some time points during treatment in patients treated with α-2a when compared to those treated with α-2b.

Conclusion: Abnormal ALT values during peg-IFN plus ribavirin treatment are observed relatively frequently, even in patients without detectable HCV RNA. Direct or indirect involvement of drugs is considered as one possible cause.

Key words: abnormal ALT values, BMI, drug involvement, pegylated interferon α-2b, ribavirin.

INTRODUCTION

THERAPEUTIC EFFORTS TO eradicate hepatitis C virus (HCV) have made outstanding progress via pegylated-interferon (peg-IFN) α plus ribavirin therapy. Sustained viral response (SVR) is achieved in about 50% of chronic viral hepatitis [CHC] patients, even with genotype 1 and high viral titers.[1–4]

One of the most frequent adverse effects of peg-IFN α plus ribavirin therapy is the elevation of alanine aminotransferase (ALT) values during treatment, which occasionally forces therapy to be discontinued,[5] as the triggering of an autoimmune mechanism by IFN has been reported to cause hepatic damage.[6,7] In addition to these rare and severe elevations of ALT, mild abnormalities during treatment are frequently observed and are recognized clinical concerns.[8–10] Because prompt viral decreases after the start of therapy primarily accompany decreases in ALT levels, the clear correlation between viral and biochemical responses is a standard pattern of therapeutic response. Thus, abnormal ALT levels during treatment are associated with the presence of HCV RNA due to a low response to therapy. However, a fairly large

Correspondence: Dr Shogo Ohkoshi, Gastroenterology and Hepatology, Graduate School of Medical and Dental Sciences Niigata University, 1-754 Asahimachi-dori, Cyuo-ku, Niigata-city, 951-8122, Japan.
Email: okoshi@med.niigata-u.ac.jp
Received 24 March 2010; revision 22 September 2010; accepted 9 November 2010.

number of patients experience elevation of ALT after the start of therapy without detectable HCV RNA in the serum. The mechanism of this phenomenon is largely unknown, and few studies have attempted to clarify the clinical parameters that affect this abnormality.[9,10]

Another concern related to the elevation of ALT values in patients during the treatment is its influence upon therapeutic outcome. Basso *et al.*[10] analyzed patients who showed viral clearance after peg-IFN plus ribavirin treatment and reported that ALT elevation in the later phases of therapy is more common in relapsing patients. Thus, whether abnormal ALT values during treatment in patients with negative HCV RNA is related to a lower probability of SVR is an important issue that needs to be clarified.

The aim of this study is to assess the incidence and severity of abnormal ALT values during peg-IFN α plus ribavirin therapy, in order to clarify the clinical parameters that may affect this phenomenon and to characterize the clinical outcome of such patients.

MATERIALS AND METHODS

Patient population

A TOTAL OF 243 CHC patients with genotype 1b who received peg-IFNα-2b plus ribavirin therapy (48 weeks in 203 patients and 72 in 32) at our affiliated institutions were enrolled, and details were gathered prospectively on a database, which was reviewed retrospectively. Eight patients were excluded from the analysis because they received treatment for less than 12 weeks due to adverse effects. Characteristics of the remaining 235 patients are shown in Table 1. The data on EVR (early viral response) and therapy outcome were available in 164 (69.8%) and 218 (92.8%) of patients, respectively. Seventeen patients (7.2%) were lost during the follow-up period and data have not been obtained. Fifty-four (23.0%) patients had abnormal ALT values during treatment. The definition of abnormal ALT values during treatment was as follows: no normalization (≥36 IU/L) during treatment (data collection points were 4, 8, 12, 24, and 48 weeks after the start of treatment [total, 5 points]) (*Criteria A*), or re-elevation of ALT (≥36 IU/L) during treatment after normalization (*Criteria B*). Individual data were considered valid when at least three of five data points were available. Clinical parameters that determine abnormal ALT values during treatment were analyzed. These include sex, age, body mass index (BMI; weight in kilograms divided by the square of height in meters), pretreatment ALT levels, hemoglobin (Hgb), white blood cell (WBC) count, platelet (Plt) count, fibrosis stage, presence of EVR, and treatment outcome. Thirty-one (13.2%) patients who discontinued beyond 12 weeks of treatment were included in the analysis by using ALT values before the stop of treatment.

Table 1 Characteristics of 235 patients with chronic hepatitis C subjected to analysis

Sex ($n = 235$)	
Male	129 (54.9%)
Female	106 (45.1%)
Age (y) (mean [±s.d]) ($n = 235$)	56.8 ± 11.0 (21–76)
Body mass index (mean [±s.d]) ($n = 221$)	23.5 (±3.5)
Histology (F stage) ($n = 119$)	
F (0–2)	96 (80.7%)
F (3–4)	23 (19.3%)
Laboratory tests ($n = 235$)	
ALT (IU/L) (mean [±s.d])	82.3 (±56.3)
WBC (/μL) (mean [±s.d])	4755 (±1458)
Hgb (g/dL) (mean [±s.d])	14.0 (±1.4)
Plt ($\times 10^4$IU/μL) (mean [±s.d])	15.6 (±5.5)
Viral load ($n = 232$)*	
Low	12 (5.2%)
High	220 (94.8%)
EVR ($n = 164$)	
+	115 (70.1%)
–	49 (29.9%)
Outcome ($n = 218$: Intention-to-treat)	
SVR	117 (53.7%)
Relapse	45 (20.6%)
Null	56 (25.7%)
ALT abnormality ($n = 235$)	
+	54 (23.0%)
–	181 (77.0%)
Discontinuation of treatment	31 (13.2%)

*High viral load is defined as more than 100 kIU/mL by Amplicore (Version 2) or 5.0 Log IU/mL by TaqMan PCR.

Because this was a multi-center study in which data were collected by fax or mailing, only a limited number of histological slides were available. A total of 25 slides were examined by a professional pathologist (M. N.), and steatosis levels were graded.[11] Four patients were scored as grade 1 and 21 were grade 0.

In order to further characterize the mechanisms involved, we also evaluated changes in ALT values in 116 patients with genotype 1b who were treated with peg-IFNα-2a plus ribavirin. Because this was a different cohort, we evaluated the data as a reference study (peg-IFNα-2b plus ribavirin), focusing on the comparison of changes of ALT values during treatment.

The studies were approved by the ethics committee of Niigata University, and were carried out in accordance with the Declaration of Helsinki. Informed consent was obtained from all patients before enrollment.

Treatment

This study was based on patients treated in routine daily practice, and thus drug dosing was left to each physician's discretion and was based on drug information, that is: Patients received peg-IFNα-2b (Pegintron; Schering-Plough, Kenilworth, NJ, USA) subcutaneously at a dosage of 1.5 μg/kg every week for 48 to 72 weeks (if viral clearance was delayed). Dose was reduced when blood neutrophil and Plt levels decreased below 750/mm^3 and 7.5×10^4/μL, respectively. Daily ribavirin (Rebetol, Schering-Plough) was given orally and the dosage was adjusted based on weight (600 mg for ≤60 kg, 800 mg for 60 to 80 kg, 1000 mg for >80 kg). Dose was also reduced when hemoglobin (Hgb) levels decreased below 10 g/dL. HCV RNA titers were measured by quantitative RT-PCR (Amplicor monitor version 2, Roche Diagnostic Systems, CA, USA). HCV RNA negativity was mainly evaluated by qualitative RT-PCR (Amplicor, Roche). HCV RNA was also quantified by Cobas TaqMan PCR assay (Roche) in some patients (28/232[12.1%]). EVR was defined as undetectable HCV RNA before or at 12 weeks of therapy. SVR was defined as undetectable HCV RNA at 24 weeks after completion of treatment. Null and relapse (both were defined as non-response; NR) were defined as positive HCV RNA during treatment, and negative HCV RNA during treatment, but showing positive HCV RNA after the completion of treatment, respectively.

Patients treated with peg-IFNα-2a received 180 μg of drug (Pegasys; Hoffman-LaRoche, Basel, Switzerland) plus ribavirin (Copegus) for 48 to 72 weeks. Dose was reduced according to drug information in a same manner as for peg-IFNα-2b. Virological evaluations were also performed in the same manner.

Statistical analysis

Chi-squared test was used to evaluate the relationship between nominal variables (sex, EVR, fibrosis level [Low: F0-2, High: F3-4], SVR), and each end-point (abnormal ALT levels during treatment or therapy outcome). Student's *t*-test was used for inter-groups comparisons of mean values. Paired Student's *t* test was used to evaluate changes in ALT values after the completion of treatment. Multivariate logistic regression analyses were used to exclude the effects of confounding variables in order to determine specific factors that may be associated with abnormal ALT values during treatment. For this analysis, ALT abnormalities were assigned as the outcome variable, and sex, age, BMI, ALT, WBC, Hgb, Plt, presence of EVR, and therapy outcome (SVR or not) were used as predictor variables (fibrosis stage was excluded because of the small number; $n = 119$). Age, WBC, Hgb, Plt values were divided into categories using the mean values, and were analyzed. Analyses were also performed in the same manner for the prediction of SVR. All analyses were performed using a statistical software package (SPSS 15.0J for Windows, Chicago, IL). All tests were two-sided, with significance set at $P < 0.05$.

RESULTS

Patient characteristics

CLINICAL BACKGROUND, LABORATORY data on CH (C) patients receiving peg-IFNα-2b plus ribavirin therapy, are shown in Table 1. One-hundred and twenty-nine of 235 patients (54.9%) were male, and 106 patients (45.1%) were female. Mean age was 56.8 years. Liver biopsy was performed in 119 (50.6%) patients. Twelve (5.1%) cases had low viral titers (≤100 k by Amplicore or 5.0 Log IU/mL TaqMan PCR). SVR was obtained in 117/218 (53.7%) patients on intention-to-treat analysis.

Fifty-four (23.0%) patients met our criteria for abnormal ALT, and of these, 45 (83.3%) met criteria A, and 9 (16.7%) met criteria B. Maximum ALT value among these patients was 226 IU/L and the mean value was 82.5 IU/L. The mean abnormal ALT level was 77.9 IU/L in the SVR or relapsed patients and 95.7 in the null patients (NS). Therapy was discontinued in one patient due to ALT elevation (maximum value was 162 IU/L). Abnormal ALT values were observed in 17 of 117 (14.5%) in patients with SVR, and 8 of 45 (17.8%) in relapse (Table 2A, lower).

Factors affecting end-points

In this study, we particularly focused on identifying clinical parameters that may be associated with abnormal ALT values during peg-IFNα-2b plus ribavirin treatment. The analyzed factors that influence this phenomenon are shown in Table 2A. Among the factors analyzed using chi-squared test or Student's *t* test, higher pretreatment ALT levels, higher BMI, higher levels of fibrosis (F3 or 4), and absence of SVR were identified as statistically significant. Among comparisons between three therapeutic outcomes (SVR, Relapse, and Null), the frequency of abnormal ALT values was significantly

Table 2 Characteristics of patients considered in comparison analysis

A) Categorized by presence of abnormal ALT values			
	Normal ($n = 181$)	Abnormal ($n = 54$)	
Male (n [%])	93 (51.4)	36 (66.7)	NS
Age (y) (mean [±s.d.])	56.7 (±11.1)	55.9 (±11.0)	NS
BMI (mean [±s.d.])	23.3 (±3.3)	24.5 (±3.2)	0.020
ALT (mean [±s.d.])	66.3 (±49.3)	109.1 (±73.2)	0.001
WBC (mean [±s.d.])	4700 (±1490)	4880 (±1263)	NS
Hgb (mean [±s.d.])	13.9 (±1.4)	14.3 (±1.4)	NS
Plt (mean [±s.d.])	15.9 (±5.6)	15.4 (±4.8)	NS
Fibrosis stage (F ≥ 3) ([%], $n = 119$)	14/96 (14.6)	9/23 (39.1)	0.017
EVR (n[%], $n = 164$)	93/129 (72.1)	22/35 (62.9)	NS
SVR (n[%], $n = 218$)	100/169 (59.2)	17/49 (34.7)	0.001
Frequency of patients with abnormal ALT in each group			
in SVR: in relapse	17/117 (14.5%) : 8/45 (17.8%)		NS
in null: in relapse	24/56 (42.9%) : 8/45 (17.8%)		0.010
B) Categorized by achievement of SVR			
	SVR ($n = 117$)	NR ($n = 101$)	
Male (n [%])	70 (59.8)	50 (49.5)	NS
Age (y) (mean [±s.d.])	55.2 (±12.1)	57.9 (±10.1)	NS
BMI(y) (mean [±s.d.])	23.5 (±3.6)	23.3 (±3.2)	NS
ALT (mean [±s.d.])	86.5 (±62.6)	76.8 (±48.3)	NS
WBC (mean [±s.d.])	5125 (±1596)	4415 (±1158)	0.003
Hgb (mean [±s.d.])	14.1 (±1.3)	13.9 (±1.5)	NS
Plt (mean [±s.d.])	16.6 (±5.5)	15.1 (±5.4)	NS
Fibrosis stage (F ≥ 3) ([%])	9/67 (13.4)	13/46 (28.3)	NS
EVR (n[%])	86/94 (91.5)	23/61 (37.7)	<0.001

higher in null patients. With regard to factors that influence SVR, significant associations were seen for EVR and low WBC counts (Table 2B). Multivariate logistic regression analysis showed that high pretreatment ALT values [$P = 0.002$, odds ratio (OR) = 1.014, 95% confidence interval (CI) = 0.875–1.175], non-SVR outcome [$P = 0.009$, 5.430, 95% CI = 4.688–6.290], and higher BMI [$P = 0.027$, OR = 1.181, 95% CI = 1.020–1.368] were significant factors associated with abnormal ALT values during treatment. The same analysis showed that EVR and normal ALT values during treatment were significant factors associated with the achievement of SVR. Changes in ALT values after the completion of treatment in patients with abnormal ALT values were analyzed (Fig. 1). ALT values gradually decreased to normal after the completion of treatment in patients with SVR, but this was not the case for NR.

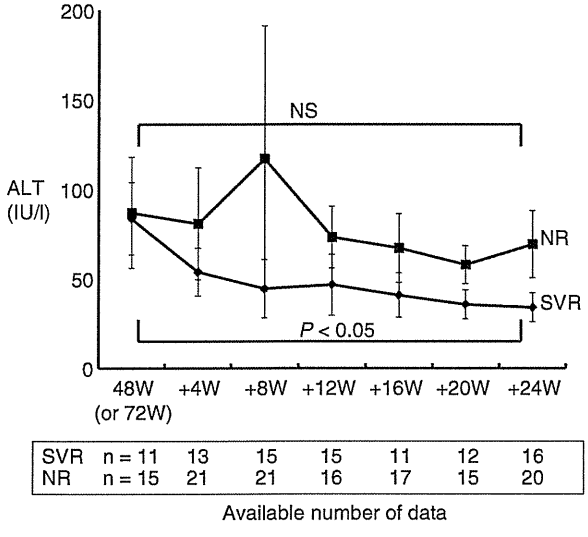

Figure 1 Changes in ALT values in NR and SVR patients during and after the completion of treatment. Mean and standard deviation values are shown. ALT values only decreased significantly in SVR patients.

Comparison with cohort treated with peg-IFNα-2a plus ribavirin

Clinical and virological factors among those who received peg-IFNα-2a plus ribavirin (age, sex, levels of

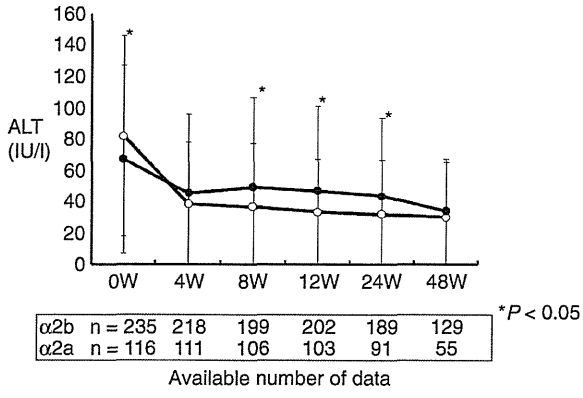

Figure 2 Comparison of ALT levels during peg-IFNα-2b plus ribavirin and peg-IFNα-2a plus ribavirin. Mean ALT values were significantly high in α-2b patients at the start of the treatment, but were significantly higher in α-2a patients at 8, 12, and 24 weeks at treatment. Number of patients for whom data was obtained is shown.

fibrosis, Hgb, WBC, Plt levels and viral load) were not different significantly from those treated with peg-IFNα-2b plus ribavirin (data not shown), except that mean ALT levels before treatment were lower (66.7 IU/L for α-2a vs. 82.1 for α-2b, $P < 0.05$). SVR was obtained in 34/55 (61.8%) of patients from whom data were available (Intention-treat analysis). A comparison of changes in ALT values before and during treatment between the two groups is shown in Figure 2. Mean ALT values were significantly higher in patients treated with α-2a when compared with those treated with α-2b at 8, 12, and 24 weeks after the start of treatment. We also performed statistical analysis after combining two individual cohorts (α-2b and α-2a). As a result, significant factors associated with abnormal ALT were male sex, use of peg-IFNα-2a, higher ALT values before treatment. Higher ALT values and peg-IFNα-2a were also identified using multivariate logistic regression analysis (BMI was not included as an index because of the low number of data).

Histological analysis

Twenty-five (25) slides prepared from pretreatment biopsy specimens were analyzed for steatosis levels. There was no relationship between the level of steatosis and mean ALT levels (103 IU/L for steatosis-grade 0 and 85.6 for grade 1). Moreover, hepatic steatosis did not have any correlation with the appearance of ALT abnormalities, that is, grade 1 hepatic steatosis was observed in 1/4 of ALT abnormalities and 5/21 without abnormalities (NS).

Two patients (60-year-old male, patient 1; and 62-year-old female, patient 2) treated with peg-IFNα plus ribavirin for 72 weeks showed continuously abnormal ALT levels (mean 141 IU/L and maximum 214 in patient 1, and 103 IU/L and 153 in patient 2) despite negative HCV RNA. In order to clarify the pathogenesis of these phenomena, liver biopsy was performed and histological comparisons with pretreatment specimens were made (Fig. 3A–D). An increase of hepatic steatosis was observed in patient 1, while marked levels of interface hepatitis with hepatocyte degeneration were observed in patient 2. Both patients were negative for anti-nuclear and anti-mitochondrial antibody, and abstinence from alcohol was confirmed. HCV RNA reappeared in both patients after the completion of treatment.

Can abnormal ALT values without detectable viraemia help to predict relapse?

We examined whether the presence of abnormal ALT values in patients who became HCV RNA-negative during treatment is a predictable marker of relapse after treatment. EVR patients treated for 48 weeks were subdivided based on the presence of abnormal ALT values during treatment in order to investigate relapse rates. The relapse rate was 28/110 (25.5%) in the normal ALT group and 4/19 (21.1%) in the abnormal group (NS).

DISCUSSION

ONE OF THE most frequent adverse effects of IFN therapy is elevation of serum ALT levels.[8–10] This phenomenon is closely associated with detectable HCV RNA attributable to unresponsiveness to therapy. However, viral response is not always associated with biochemical response, so this is often observed in patients without detectable HCV RNA.[12,13] Although this non-specific elevation of ALT had been seen since the era of regular interferon treatment for CHC,[8] it appears to be more frequently observed since the start of peg-IFN treatment. To date, few reports have attempted to assess the frequency and define factors associated with elevated serum ALT,[9,10] and currently there have been no reports in Japanese populations. In addition, we recently experienced a female patient who was treated with peg-IFNα-2a plus ribavirin, and who showed continuously abnormal ALT values during treatment with no detectable HCV RNA. She eventually developed liver cirrhosis (Case report [In Press, Nippon Shokakibyo Gakkai Zasshi], and she is patient 2 in Figure 3C and D). These clinical experiences led to concerns over whether

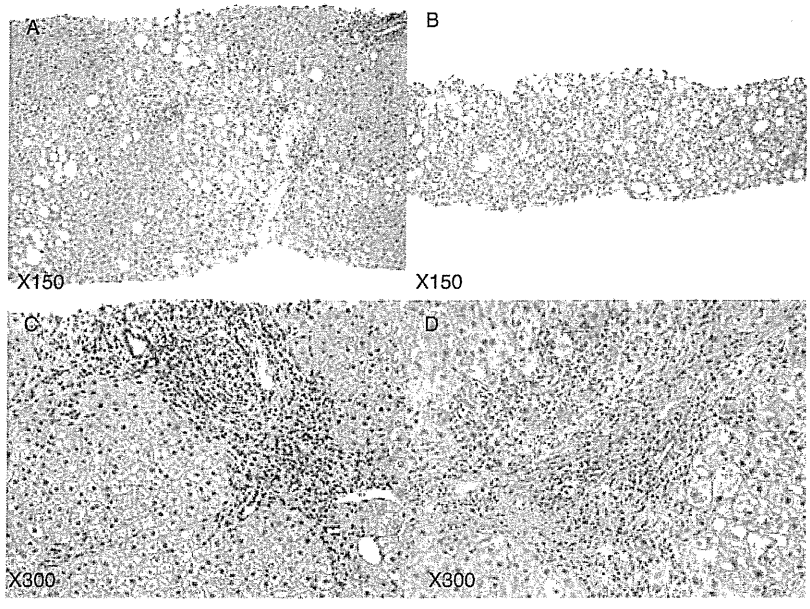

Figure 3 Two patients (60-year-old male, patient 1; and 62-year-old female, patient 2) treated with peg-IFNα plus ribavirin for 72 weeks, showed continuously abnormal ALT levels (mean 141 IU/L and maximum 214 IU/L in patient 1; 103 IU/L and 153 IU/L) despite undetectable HCV RNA (HCV RNA became negative at 20 and 16 weeks after the start of treatment, respectively. Pretreatment liver biopsy showed steatosis and mild inflammation in portal area in patient 1 (A), and a moderate level of inflammation in portal area in patient 2 (C). Liver biopsies were performed at 48 weeks during treatment in patient 1 and after 4 months of treatment completion in patient 2. Reduced inflammation and increased steatosis were observed were observed in patient 1 (B). Severe necroinflammation with interface hepatitis and hepatocyte degeneration were observed in patient 2 (D). Original magnification is shown.

non-specific elevation of ALT during treatment can have detrimental clinical impact on patients treated with peg-IFN plus ribavirin. Thus, we attempted to clarify its incidence, severity, and clinical background.

We first included patients with all treatment response patterns in the analysis. The frequency of ALT elevation during treatment was 23.0% in our study. Thurairajah *et al.* reported that it occurred in 35% of patients treated with peg-IFN plus ribavirin.[9] This difference may have been due to the definition of abnormal ALT levels; they defined abnormal levels as any rise above baseline, while in our study, patients who had abnormal ALT during the first treatment period but that gradually normalized later were not counted. There was just one patient in our cohort who discontinued therapy due to ALT elevation (162 IU/L). Otherwise, this phenomenon was not the main reason for discontinuing treatment.

On multivariate logistic regression analysis, higher pretreatment ALT levels, BMI, and non-SVR rate were significantly and independently associated with abnormal ALT during treatment. Of two previous reports that analyzed the relationship between elevation of ALT during treatment and clinical parameters, one showed no associated parameters,[10] and the other found associations with body weight and steatosis.[9] These differences may be due to differences in cohort and patient ethnicity. Interestingly, higher levels of pretreatment ALT and BMI did not have significant associations with therapy outcome in our study, but were associated with abnormal ALT values (Table 2B). Our results were not apparently consistent with a previous observation showing that high BMI is an independent risk factor of non-response with IFN[14]. This discrepancy may be because our cohort included only a small number of patients with BMI of ≥30 for whom non-responsiveness to therapy was seen.[14]

Positive associations between overweight and hepatic dysfunction by anti-cancer drugs have been reported.[15] Obesity affects anti-cancer agents by reducing clearance, prolonging the elimination half-life, and increasing the area under the plasma concentration-time curve.[16,17] Altered pharmacokinetics due to body fat volume may

cause hepatic dysfunction.[18] Based on these previous findings, we speculate that altered pharmacokinetics due to the volume of fat mass, to some extent, are involved in the positive association between high BMI and elevated ALT values during therapy in patients being treated with peg-IFN plus ribavirin.

High pretreatment ALT value, which is another significant factor associated with abnormal ALT values during treatment, might be due to carry-over of pre-existing pathogenic conditions, such as hepatic steatosis, that are frequently observed in CHC.[19,20] Unexpectedly, pretreatment ALT values had no clear correlation with BMI ($r = 0.017$) in our cohort. In addition, although the number of samples was limited ($n = 25$), there was no relationship between the levels of steatosis and mean ALT levels, and hepatic steatosis did not show any correlation with the appearance of ALT abnormalities. Thus, the relationship between hepatic steatosis and ALT abnormalities remains unknown.

What is the pathogenetic mechanism responsible for elevation of ALT during treatment, particularly in patients who became negative for HCV RNA during treatment? The results of paired biopsy from two patients with abnormal ALT values during treatment despite having undetectable HCV RNA are shown Figure 3. Patient 1 showed an increase in steatosis, while patient 2 showed severe necroinflammation and hepatocyte degeneration. Pathological findings of drug induced liver injury are various, and these findings may be compatible with one of those.[21] Because the pathological findings were different between two patients treated with same drugs, we speculate that the pathogenesis of these ALT abnormalities is composed of multiple factors such as genetic or immunological. Recently, Nagashima *et al.* showed a significant correlation between elevated ALT and serum ferritin levels during peg-IFN treatment.[22] We note that serum ferritin levels increased in both patients after the start of treatment.

We performed a longitudinal comparison of ALT values after the completion of treatment between SVR and null-relapse patients in order to address the pathogenesis of elevated ALT (Fig. 1). While ALT values decreased significantly to normal levels in the SVR patients, they did not change in the viraemic (null or relapse) patients. This shows that the abnormal ALT levels during treatment without detectable viraemia diminished after the completion of therapy in SVR patients, thus suggesting that a pre-existing condition associated with HCV, such as hepatic fibrosis, might have been resolved with successful therapy. It is more likely, however, that abnormal ALT levels during treatment without detectable viraemia is partly attributable to the direct or indirect effects of drugs.

We showed that ALT levels during treatment were significantly higher in patients treated with peg-IFNα-2a plus ribavirin than in those treated with peg-IFNα-2b plus ribavirin at some time points, despite similar therapeutic outcomes (Fig. 2). In addition to the differences in IFN molecular species, particularly the difference in their molecular weights, result in distinct half-lives (peg-IFN α-2a: longer half-life, peg-IFN α-2b: shorter half life[23]) which may explain this phenomenon. We speculate that abnormal ALT levels in patients during treatment are partially caused by the treatment itself (presumably IFN), possibly being affected by the delayed clearance from the body due to pegylation, and this would be more evident in patients with high BMI.

Clinically, it is important to determine whether the presence of abnormal ALT values in patients who became HCV RNA-negative during treatment is a predictable marker of relapse after treatment. However, we were unable to confirm whether abnormal ALT during treatment is significantly associated with a greater risk of relapse. On the other hand, Basso *et al.*[10] reported that ALT elevation in the later phases of therapy is more common in relapsing patients. Thus, patients with abnormal ALT who became negative for HCVRNA during treatment were classified into two groups depending on the time of peak ALT (i.e. ≤ 12; early elevation; or > 12 weeks, late elevation). Among the data available, 9/12 (75%) patients with early elevation and 6/12 (50%) with late elevation achieved SVR. Although not significant, the trend seems to be analogous to Basso's report. However, a large data set is necessary to confirm the result.

In conclusion, the direct or indirect effects of peg-IFN plus ribavirin may partly explain the non-specific elevation of ALT levels during treatment. Although most increases are mild, careful observation and consideration of the potential threat to clinical course are necessary.

REFERENCES

1 Hayashi N, Takehara T. Antiviral therapy for chronic hepatitis C: past, present, and future. *J Gastroenterol* 2006; 41: 17–27.
2 Omata M, Yoshida H, Shiratori Y. Prevention of hepatocellular carcinoma and its recurrence in chronic hepatitis C patients by interferon therapy. *Clin Gastroenterol Hepatol* 2005; 10 (Suppl 2): S141–3.

3 Zeuzem S. Interferon-based therapy for chronic hepatitis C: current and future perspectives. *Nat Clin Pract Gastroenterol Hepatol* 2008; **5**: 610–22.
4 Heathcote EJ. Antiviral therapy: chronic hepatitis C. *J Viral Hepat* 2007; **14** (Suppl 1): 82–8.
5 Cervoni J-P, Degos F, Marcellin P, Erlinger S. Acute hepatitis induced by interferon, associated with viral clearance, in chronic viral hepatitis. *J Hepatol* 1997; **27**: 1113–16.
6 Kogure T, Ueno Y, Fukushima K *et al.* Fulminant hepatic failure in a case of autoimmune hepatitis in hepatitis C during peg-interferon-alpha 2b plus ribavirin treatment. *World J Gastroenterol* 2007; **13**: 4394–7.
7 Sezaki H, Arase Y, Tsubota A *et al.* Type C-chronic hepatitis patients who had autoimmune phenomenon and developed jaundice during interferon therapy. *J Gastroenterol* 2003; **38**: 493–500.
8 Dusheiko G. Side effects of alpha interferon in chronic hepatitis. *Hepatology* 1997; **26** (Suppl 1): 112S–21S.
9 Thurairajah PH, Thorburn D, Hubsher S *et al.* Incidence and characterization of serum transaminases elevations in pegylated interferon and ribavirin treated patients with chronic hepatitis C. *Aliment Phamacol Ther* 2007; **25**: 1293–300.
10 Basso M, Edoardo G, Torre F, Blanchi S, Savarino V, Picciotto A. Elevations in alanine aminotransferase levels late in the course of anti-viral therapy in hepatitis C virus RNA-negative patients are associated with virological relapse. *Hepatology* 2009; **49**: 1442–8.
11 Kleiner DE, Brunt EM, Natta MV *et al.* Design and validation of a histological scoring system for nonalcoholic fatty liver disease. *Hepatology* 2005; **41**: 1313–21.
12 Hung CH, Lee CM, Lu SN *et al.* Is delayed normalization of alanine aminotransferase a poor prognostic predictor in chronic hepatitis C patients treated with a combined interferon and ribavirin therapy? *J Gastroentarol Hepatol* 2002; **17**: 1307–11.
13 Zeuzem S, Feinman SV, Rasenack J *et al.* Peginterferon alpha-2a in patients with chronic hepatitis C. *N Engl J Med* 2000; **343**: 1666–72.
14 Bressler BL, Guindi M, Tomlinson G, Heathcoate J. High body mass index is an independent risk factor for nonresponse to antiviral treatment in chronic hepatitis C. *Hepatology* 2003; **38**: 639–44.
15 Fujiwara Y, Kiura K, Hotta K, Tabata M, Takikawa N, Tanimoto M. Being overweight influences the development of hepatic dysfunction in Japanese patients with non-small-cell lung cancer undergoing cytotoxic chemotherapy. *Lung Cancer* 2007; **55**: 343–8.
16 Rodvold KA, Rushing DA, Tewksbury DA. Doxorubicin clearance in the obese. *J Clin Oncol* 1988; **6**: 1321–7.
17 Lind MJ, Margison JM, Cerny T, Thacher N, Wilkinson PM. Prolongation of isosfamide elimination half-life in obese patients due to altered drug distribution. *Cancer Chemother Pharmacol* 1989; **25**: 139–42.
18 Cheymol G. Effects of obesity on pharmacokinetics implications for drug therapy. *Clin Phamacokinet* 2000; **39**: 215–31.
19 Koike K, Moriya K. Metabolic aspects of hepatitis C virus infection: steatohepatitis resembling but distinct from NASH. *J Gastroenterol* 2005; **40**: 329–36.
20 Sheikh MY, Choi J, Qadri I, Friedman JE, Sanyal AJ. Hepatitis C virus infection: molecular pathways to metabolic syndrome. *Hepatology* 2008; **47**: 2127–33.
21 Scheuer JP, Lefkowitch JH. *Liver Biopsy Interpretation*, 7th edn. Burlington: Elsevier Saunders, 2006; 125–44.
22 Nagashima M, Kudo M, Chung H *et al.* Elevated serum ALT levels during pegylated interferon monotherapy may be caused by iron overload. *Intervirology* 2008; **51** (Suppl 1): S76–85.
23 Webster R, Didier E, Harris P *et al.* Pegylated proteins: evaluation of their safety in the absence of definitive metabolism studies. *Drug Metab Dispos* 2007; **35**: 9–16.

World Journal of Hepatology

Online Submissions: http://www.wjgnet.com/1948-5182office
wjh@wjgnet.com
doi:10.4254/wjh.v3.i1.15

World J Hepatol 2011 January 27; 3(1): 15-23
ISSN 1948-5182 (online)

BRIEF ARTICLE

Multicentric occurrence of hepatocellular carcinoma with nonalcoholic steatohepatitis

Hirokazu Kawai, Minoru Nomoto, Takeshi Suda, Kenya Kamimura, Atsunori Tsuchiya, Yasushi Tamura, Masahiko Yano, Masaaki Takamura, Masato Igarashi, Toshifumi Wakai, Satoshi Yamagiwa, Yasunobu Matsuda, Shogo Ohkoshi, Isao Kurosaki, Yoshio Shirai, Masahiko Okada, Yutaka Aoyagi

Hirokazu Kawai, Department of Clinical Laboratory, Niigata University Medical and Dental Hospital, Niigata 951-8510, Japan
Minoru Nomoto, Takeshi Suda, Kenya Kamimura, Atsunori Tsuchiya, Yasushi Tamura, Masahiko Yano, Masaaki Takamura, Masato Igarashi, Satoshi Yamagiwa, Shogo Ohkoshi, Yutaka Aoyagi, Division of Gastroenterology and Hepatology, Niigata University Graduate School of Medical and Dental Sciences, Niigata 951-8510, Japan
Toshifumi Wakai, Isao Kurosaki, Yoshio Shirai, Division of Digestive and General Surgery, Niigata University Graduate School of Medical and Dental Sciences, Niigata 951-8510, Japan
Yasunobu Matsuda, Department of Medical Technology, Niigata University Graduate School of Health Sciences, Niigata 951-8518, Japan
Masahiko Okada, Division of Preventive Medicine, Niigata University Graduate School of Medical and Dental Sciences, Niigata 951-8510, Japan
Author contributions: Kawai H is a physician who drafted the manuscript and revised critically for content; Nomoto M contributed to the pathological analysis; Suda T was a major contributor to writing the manuscript; Kamimura K, Tsuchiya A, Tamura Y, Yano M, Takamura M, Igarashi M, Yamagiwa S, Matsuda Y, Ohkoshi S and Aoyagi Y are physicians who have treated the patients and analyzed the data; Wakai T, Kurosaki I and Shirai Y are surgeons who treated the patients; and Okada M contributed to the analysis of the data.
Correspondence to: Hirokazu Kawai, MD, PhD, Department of Clinical Laboratory, Niigata University Medical and Dental Hospital, 1-757 Asahimachi-dori Chuo-ku, Niigata 951-8510, Japan. kawaih@med.niigata-u.ac.jp
Telephone: +81-25-2272336 Fax: +81-25-2230996
Received: September 3, 2010 Revised: November 11, 2010
Accepted: November 18, 2010
Published online: January 27, 2011

Abstract

AIM: To reveal the manner of hepatocellular carcinoma (HCC) development in patients with nonalcoholic steatohepatitis (NASH) focusing on multicentric occurrence (MO) of HCC.

METHODS: We compared clinicopathological characteristics between patients with and without MO of HCC arising from NASH background. The clinical features were implicated with reference to the literature available.

RESULTS: MO of HCC was identified with histological proof in 4 out of 12 patients with NASH-related HCC (2 males and 2 females). One patient had synchronous MO; an advanced HCC, two well-differentiated HCCs and a dysplastic nodule, followed by the development of metachronous MO of HCC. The other three patients had multiple advanced HCCs accompanied by a well-differentiated HCC or a dysplastic nodule. Of these three patients, one had synchronous MO, one had metachronous MO and the other had both synchronous and metachronous MO. There were no obvious differences between the patients with or without MO in terms of liver function tests, tumor markers and anatomical extent of HCC. On the other hand, all four patients with MO of HCC were older than 70 years old and had the comorbidities of obesity, type 2 diabetes mellitus (T2DM), hypertension and cirrhosis. Although these conditions were not limited to MO of HCC, all the conditions were met in only one of eight patients without MO of HCC. Thus, concurrence of these conditions may be a predisposing situation to synchronous MO of HCC. In particular, old age, T2DM and cirrhosis were suggested to be prerequisite for MO because these factors were depicted in common among two other cases with MO of HCC under NASH in the literature.

CONCLUSION: The putative predisposing factors and necessary preconditions for synchronous MO of HCC in NASH were suggested in this study. Further investigations are required to clarify the accurate prevalence and predictors of MO to establish better strategies for treatment and prevention leading to the prognostic improvement in NASH.

Key words: Nonalcoholic steatohepatitis; Hepatocellular carcinoma; Multicentric occurrence

Peer reviewers: Sonia Ramos, PhD, Department of Metabolism and Nutrition, Instituto del Frio (CSIC), Jose Antonio Novais, Madrid 28040, Spain; Stefan Rose-John, Director, Department of Biochemistry, Christian-Albrechts-Universität zu Kiel, Medical Faculty, Olshausenstraäe 40, Kiel D24098, Germany; Johanna Kassiani Delladetsima, Associate Professor, Department of Pathology, Medical School, University of Athens, Goudi, Athens 11527, Greece

Kawai H, Nomoto M, Suda T, Kamimura K, Tsuchiya A, Tamura Y, Yano M, Takamura M, Igarashi M, Wakai T, Yamagiwa S, Matsuda Y, Ohkoshi S, Kurosaki I, Shirai Y, Okada M, Aoyagi Y. Multicentric occurrence of hepatocellular carcinoma with nonalcoholic steatohepatitis. *World J Hepatol* 2011; 3(1): 15-23 Available from: URL: http://www.wjgnet.com/1948-5182/full/v3/i1/15.htm DOI: http://dx.doi.org/10.4254/wjh.v3.i1.15

INTRODUCTION

With the increasing prevalence of obesity and type 2 diabetes mellitus (T2DM), nonalcoholic fatty liver disease (NAFLD) has become pandemic, particularly in developed countries, causing public health problems. Within the broad spectrum of the pathophysiology of NAFLD, nonalcoholic steatohepatitis (NASH) is the most serious form because of its propensity to progress toward a fatal event. Although NASH was previously thought to be often indolent[1,2], the following analyses revealed that NASH leads to fibrosis of the liver, cirrhosis and eventually hepatocellular carcinoma (HCC) in a substantial number of patients[3-7]. HCC is currently regarded as a late complication of NASH according to a number of recent reports[3-7]. In addition, it was recently shown that the development of HCC is associated with mortality in cirrhotic NASH in a prospective study in Japanese cohort[5]. Thus, it is very important to elucidate the natural course of NASH in terms of the development of HCC for better management.

Multicentric occurrence (MO) and intrahepatic metastasis (IM) are characteristic in the development of HCC with chronic liver diseases that are caused by hepatitis B virus (HBV) or hepatitis C virus (HCV)[8-13]. It is very important to distinguish MO from IM so that appropriate treatment options may be selected in a variety of clinical settings. Unfortunately, there have been few studies that focus on the characterization of MO in NASH-related HCC despite the increasing number of case reports on HCC based on NASH.

In this report, characteristic features of NASH cases that developed HCC with MO are discussed.

MATERIALS AND METHODS

Patients

From July 2002 to March 2010, we diagnosed and treated 40 adult patients with NASH at the Division of Gastroenterology and Hepatology, Niigata University Medical and Dental Hospital. Of these, HCC was observed in 12 cases including 4 with MO of HCC. The proportion of HCC patients is high in our series with NASH because our hospital is a tertiary referral center and most of the NASH patients who are referred to us are complicated cases.

Definitions

NASH was defined to satisfy all of the following requirements: (1) an absence of clinically significant alcohol intake (less than 20 g/d of ethanol consumption); (2) histological features showing steatosis with various combinations of ballooning liver cells, inflammatory infiltrate of neutrophils, pericellular fibrosis and Mallory bodies; and (3) no other liver diseases. All non-tumorous specimens were histologically scored according to the classification by Brunt *et al*[14].

MO of HCC was pathologically determined according to the classification of the Liver Cancer Study Group of Japan[15] as follows: 2 or more separate lesions including an early HCC with a dysplastic nodule or no substantial destruction of the preexisting hepatic framework, or moderately and/or poorly differentiated HCCs with a margin of well-differentiated HCC. When histological specimens of HCC could not be obtained, MO was identified by particular findings that correspond to MO on imaging studies[16,17].

Advanced HCCs were defined when they had a vascular pattern that was consistent with contrast enhancement in the arterial phase followed by rapid washout in the portal and/or equilibrium phases on dynamic computed tomography (CT) and/or dynamic magnetic resonance (MR) imaging. A nodule was also diagnosed with an advanced HCC when the lesion was depicted as a defect on CT during arterial portography (CTAP) and as a hyperattenuated lesion in the first phase of double-phase CT during hepatic arteriography (CTHA) followed by corona-like enhancement in the second phase[16,17]. A nodule-in-nodule appearance on dynamic CT, dynamic MR imaging or CTHA was regarded as a specific finding that indicated the emergence of a dedifferentiated component (moderately or poorly differentiated HCC) within a well-differentiated HCC, even without histological proof. Otherwise, well-differentiated HCCs or dysplastic nodules were diagnosed based on histological examinations.

The clinical stage of HCC was stratified according to the TNM classification of the Liver Cancer Study Group of Japan[18].

Obesity was defined as body mass index (BMI) $\geqslant$ 25 kg/m^2 according to the criteria proposed by the Japan Society for the Study of Obesity[19]. The definition was based on the fact that obesity-related diseases increase with BMI $\geqslant$ 25 kg/m^2 in the Japanese population. T2DM was diagnosed according to the criteria advocated by the Japan Diabetes Society as follows: fasting plasma glucose $\geqslant$ 126 mg/dL, random plasma glucose $\geqslant$ 200 mg/dL

Table 1 Clinical characteristics of patients with nonalcoholic steatohepatitis-related hepatocellular carcinoma with or without multicentric occurrence

	HCC with MO				HCC without MO							
Case	1	2	3	4	5	6	7	8	9	10	11	12
Age at Dx of NASH	73	81	78	71	68	75	71	80	75	78	81	66
Gender	F	M	M	F	M	F	M	F	F	M	M	M
History of BTF	-	-	-	-	-	-	-	+	-	-	-	-
BMI (kg/m^2)	31.0	26.3	25.5	32.0	26.8	23.0	27.0	32.1	34.0	23.1	24.5	25.2
T2DM	+	+	+	+	-	+	+	-	+	-	-	-
Hypertension	+	+	+	+	-	-	-	+	+	-	+	+
Dyslipidemia	-	-	-	+	-	+	+	+	-	+	+	-
Varices	-	-	-	-	+	-	+	-	+	-	-	-
Ascites	-	-	-	-	-	-	-	-	-	-	-	-
AST (IU/L)	91	67	43	33	34	43	36	34	43	25	83	78
ALT (IU/L)	46	48	49	21	17	32	22	33	40	20	37	75
γ-GTP (IU/L)	122	129	418	72	30	222	46	67	73	104	360	279
Total bilirubin (mg/dL)	1.0	0.7	0.8	1.1	1.4	1.1	1.5	0.6	1.2	0.6	0.6	0.8
Albumin (g/dL)	3.8	3.7	3.4	2.9	3.3	4.0	2.9	4.1	3.7	3.8	3.4	4.2
Prothrombin time (%)	53	72	97	62	69	NA[a]	59	69	86	75	84	NA[a]
Platelet (× 10^4/μL)	21.1	12.3	10.4	11.2	4.5	14.5	6.4	31.6	11.7	12.1	26.4	11.4
Child-Pugh score	A	A	A	B	B	-[a]	B	A	A	A	A	-[a]
HBsAg	-	-	-	-	-	-	-	-	-	-	-	-
Anti-HBc	+	-	-	+	-	-	-	-	+	+	-	+
Anti-HCV	-	-	-	-	-	-	-	-	-	-	-	-
Histological features (Classification by Brunt)												
Grade	2	2	2	2	1	2	2	1	1	1	2	2
Stage	4	4	4	4	4	4	4	4	4	1	2	4
Type of cirrhosis	Mixed	Mixed	Macro	Mixed	Micro	Mixed	Mixed	Mixed	Mixed	-	-	Macro
AFP (ng/mL)	11	26	15	25	7	9	3	8 757	12	2 963	900 100	8
DCP (mAU/mL)	18	24	20	116	24	NA[a]	14	35	907	131	10 700	NA[a]
Maximum size of HCC (mm)	35	50	40	28	22	17	50	26	40	40	110	70
Number of HCC	Mul	Mul	Mul	Mul	Mul	Sol	Mul	Sol	Mul	Mul	Mul	Sol
TNM stage	Ⅲ	Ⅲ	Ⅲ	Ⅲ	ⅣA	Ⅰ	Ⅲ	Ⅱ	Ⅲ	ⅣB	Ⅲ	Ⅱ
Initial treatment	Ope	TACE + RFA	Ope	TACE + RFA	TAI	RFA	TACE	TACE + Ope	Ope + RFA	Chemo	Ope	TAI + Ope
Outcome	Alive	Dead	Dead	Alive	Alive	Alive	Alive	Alive	Dead	Dead	Alive	Alive
Cause of death	-	LR	NLR	-	-	-	-	-	LR	LR	-	-
Follow-up period after Dx of HCC (days)	2 599	1 706	288	1 140	280	1 011	687	2 198	1 525	489	162	330

HCC: hepatocellular carcinoma; MO: multicentric occurrence; Dx: diagnosis; BTF: blood transfusion; BMI: body mass index; M: Male; F: Female; T2DM: type 2 diabetes mellitus; AST: aspartate aminotransferase; ALT: alanine aminotransferase; γ-GTP: γ-glutamyltranspeptidase; NA: not available; AFP: alpha-fetoprotein; DCP: des-γ-carboxy-prothrombin; Mixed: mixed nodular cirrhosis; Macro: macronodular cirrhosis; Micro: micronodular cirrhosis; Mul: multiple; Sol: solitary; TACE: transcatheter arterial chemoembolization; TAI: transcatheter arterial infusion chemotherapy; RFA: radiofrequency ablation; Ope: operation; LR: liver-related death; NLR: non-liver-related death; [a]An oral administration of warfarin prevented the evaluation.

or hemoglobin $A_{1c} \geq 6.5\%$ on two separate occasions. The diagnosis of hypertension was made if the patient was on antihypertensive medication or had blood pressure $\geq 140/90$ mmHg on at least two separate occasions. Dyslipidemia was defined as total cholesterol level ≥ 220 mg/dL and/or fasting triglyceride level ≥ 150 mg/dL on at least two separate occasions or continuously receiving lipid-lowering agents.

Laboratory examinations

The following laboratory tests were recorded at diagnosis of HCC in all patients: aspartate aminotransferase (AST), alanine aminotransferase (ALT), γ-glutamyltranspeptidase (γ-GTP), total bilirubin, albumin, prothrombin time, platelet count, Child-Pugh score, hepatitis B surface antigen (HBsAg), hepatitis B core antibody (anti-HBc), HCV antibody (anti-HCV), alpha-fetoprotein (AFP) and des-γ-carboxy-prothrombin (DCP).

RESULTS

The clinical and laboratory data from 12 patients with NASH-related HCC are shown in Table 1. Of these, MO of HCC was observed in cases 1 to 4. Regarding common characteristics, all 4 patients with MO were over 70 years old, obese and had T2DM, hypertension and cirrhosis. Although these conditions were not limited to MO of HCC, all the conditions were met in only one (case 9) of eight patients without MO of HCC. There were no obvious differences between the patients with or without MO in terms of liver function tests, tumor markers and stages of tumor development. Although a few patients had positive anti-HBc, the titer of the antibody was low and no attribution of HBV infection to background liver disease was histologically ascertained.

The clinical courses of the 4 patients with MO of HCC are detailed below.